



Spring extratropical cyclones over the Mongolian region in the ERA5 reanalysis: climatology and variability

Kai Wang^{1,2} · Jianqi Sun^{1,2} · Yanbo Nie^{1,2}

Received: 12 May 2024 / Accepted: 23 July 2024

© The Author(s), under exclusive licence to Springer-Verlag GmbH Germany, part of Springer Nature 2024

Abstract

Mongolian extratropical cyclones (ETCs) play a crucial role in the weather and climate over East Asia, and the use of datasets with higher spatiotemporal resolutions can improve the understanding of Mongolian ETCs. Based on an automatic detection and tracking algorithm and the European Centre for Medium-Range Weather Forecasts (ECMWF) Reanalysis version 5 (ERA5) dataset, the characteristics of the frequency, lifetime, moving distance, moving speed, and intensity of Mongolian ETCs in spring during 1979–2021 are investigated. The results show that 92.6% of the Mongolian ETCs are locally formed. There were two decadal changes in the Mongolian ETC frequency in approximately 1993 and 2004, showing a “high–low–high” variation. In terms of ETC passages, there is an increasing trend from central Mongolia to Northeast China and a decreasing trend east of Lake Baikal, indicating that the Mongolian ETC tracks are located more southward. Based on the standard deviation ellipse method and K-means clustering, the Mongolian ETCs are clustered into three categories, namely, southern track (ST, accounting for 53.4% of Mongolian ETCs) ETCs, northern track (NT, accounting for 43.8%) ETCs, and long track (LT, accounting for 2.8%) ETCs. The ST ETCs have a significant increasing trend, while the NT ETCs show a significant decreasing trend. Moreover, the other properties of Mongolian ETCs also show significant decadal variability. The sequences of lifetime, moving distance, moving speed and intensity exhibit decadal changes in the 1990s, with longer lifetime and moving distance, faster moving speed, and stronger intensity after the abrupt change.

Keywords Mongolian extratropical cyclones · Classification · Cyclone properties · ERA5 reanalysis

1 Introduction

Extratropical cyclone (ETC) is an important atmosphere system at middle and high latitudes, playing a key role in transporting heat, momentum and water vapor (Chang et al. 2002; Neu et al. 2013; Reale et al. 2019; Yang et al. 2021; Messmer and Simmonds 2021). In addition, ETCs have a considerable influence on weather and climate. For example, ETCs can generally cause intense precipitation, low temperature, strong winds, dust weather and freshwater fluxes (Qian et al. 2002; Takemi and Seino 2005; Hawcroft et al. 2012; Papritz et al. 2014; Pfahl and Sprenger 2016; Li et al.

2019; Lin et al. 2019; Hirata 2021; Messmer and Simmonds 2021; Owen et al. 2021; Bueh et al. 2022; Yin et al. 2022; Yu et al. 2022). Therefore, it is important to investigate the variations in ETCs.

The identification of ETCs relies on detection and tracking algorithms, which have been widely developed in recent decades. Early ETC analysis mainly depended on manual work (Wang 1963; Chung et al. 1976; Whittaker and Horn 1984; Chen et al. 1991), after which automatic recognition algorithms were gradually developed (Murray and Simmonds 1991; Hodges 1995; Sinclair 1997; Wernli and Schwierz 2006; Ullrich and Zarzycki 2017; Ullrich et al. 2021). The automatic algorithms generally use two metrics to define cyclones, i.e., the local minimum of mean sea level pressure (MSLP) or the local maximum of vorticity. The MSLP method pays more attention to the mass field and represents more low-frequency signals, while small-scale or weak ETCs in the genesis and lysis stages may be omitted. The vorticity method is related to the wind field structure, including more high-frequency

✉ Jianqi Sun
sunjq@mail.iap.ac.cn

¹ Nansen-Zhu International Research Centre, Institute of Atmospheric Physics, Chinese Academy of Sciences, Beijing 100029, China

² University of Chinese Academy of Sciences, Beijing 100049, China

signals, but the detected ETC centers could be inconsistent with the minimum of air pressure (Hoskins and Hodges 2002; Hodges et al. 2003; Neu et al. 2013; Varino et al. 2019). Besides, Murray and Simmonds (1991), Simmonds et al. (1999), and Pezza et al. (2008) developed algorithms that consider both the pressure field and vorticity field; these algorithms have been widely used recently (Pinto et al. 2005; Zhang et al. 2012; Ulbrich et al. 2013; Chen et al. 2017; Messmer and Simmonds 2021).

East Asia is one of the high-frequent ETC centers in the Northern Hemisphere (Pinto et al. 2005; Neu et al. 2013; Rudeva et al. 2014; Yu et al. 2022). As a key member of East Asian ETCs, Mongolian ETCs are strongly linked with the weather and climate over East Asia, generally bringing low temperature, dust weather, and strong winds throughout the region (Qian et al. 2002; Yao et al. 2003; Zhu et al. 2008; Jin et al. 2021; Bueh et al. 2022; Yin et al. 2022). Spring is the most active season for Mongolian ETCs (Adachi and Kimura 2007; Wang et al. 2009; Lee et al. 2020). Previous studies have documented the temporal and spatial changes in spring Mongolian ETCs. For example, Qian et al. (2002) indicated that spring Mongolian ETCs showed an increasing trend from the 1950s to the early 1960s but then a decreasing trend until the end of the twentieth century. Yao et al. (2003) reported that the frequency of spring Mongolian ETCs was relatively low in the 1950s, high from the 1960s to the late 1970s, and low again until the end of the twentieth century. Zhu et al. (2008) reported that the low frequency of spring Mongolian ETCs continued until the early twenty-first century. Recently, Huang et al. (2016) reported that the frequency of spring Mongolian ETCs increased from the early 1960s to the late 1970s, decreased from the early 1980s to the late 1990s, and then increased slightly after 2000.

To our knowledge, most previous studies have focused on changes in Mongolian ETC frequency; in contrast, few studies have elucidated changes in the lifetime, moving distance, and moving speed of Mongolian ETCs, which are also important properties of ETCs. For example, the moving speed is closely related to the influence of ETCs: the slower the moving speed is, the greater the influence. Therefore, investigating these properties is beneficial for better understanding Mongolian ETCs. Moreover, the resolution of the data used in previous studies is relatively coarse (e.g., 2.5-degree or 1.0-degree in spatial resolution and daily or 6-hourly in temporal resolution), which may lead to inaccurate identification of the ETC center position or identification omission (Wang et al. 2016; Crawford et al. 2021; Zhong et al. 2023). The European Centre for Medium-Range Weather Forecasts (ECMWF) Reanalysis version 5 (ERA5) is the most recent reanalysis dataset of the ECMWF and has high temporal and spatial resolution (Hersbach et al. 2020). Thus, we chose ERA5 dataset (0.25-degree in spatial

resolution and 3-hourly in temporal resolution) to study the spring Mongolian ETCs in this paper.

The rest of this article is arranged as follows. Section 2 describes the data and methods used in this study, Sect. 3 presents the characteristics of Mongolian ETCs, and Sect. 4 discusses the clustering of Mongolian ETCs and the characteristics of their properties. Finally, the discussion and conclusion are presented in Sect. 5.

2 Data and method

2.1 Data

In this study, the European Centre for Medium-Range Weather Forecasts Reanalysis version 5 (Hersbach et al. 2020) dataset are used. The main field used for ETC detection and tracking is MSLP. Previous studies have suggested that data with 1-hourly temporal resolution could lead to unreasonable splitting of ETC tracks; while there are relatively few cases of track splitting at 3-hourly and 6-hourly resolution (Crawford et al. 2021). Another recent study (Zhong et al. 2023) also suggested that the lifetime and moving distance of 3-hourly resolution dataset are always greater than those of 1-hourly and 6-hourly resolution, indicating that track splitting is relatively less at 3-hourly resolution. Therefore, basing on these previous studies, we chose 0.25-degree in spatial resolution and 3-hourly in temporal resolution to study the spring Mongolian ETCs in this paper. In addition, physical fields include zonal and meridional winds, geopotential height, air temperature and potential vorticity at pressure levels are also used in analysis.

The reproducibility of MSLP in the ERA5 dataset is evaluated by comparing with HadSLP2. The HadSLP2 is a combination of monthly globally-complete fields of land and marine pressure observations on a 5-degree latitude–longitude grid from 1850 to 2004 (Allan and Ansell 2006). The common period (1979–2004) of the two datasets is selected for analysis (figure not shown). The spatial correlation between MSLP climatology based on ERA5 (interpolated to 5-degree latitude–longitude grid) and MSLP climatology based on HadSLP2 is 0.84 ($P < 0.01$), and the correlation coefficient of area-averaged MSLP sequences in ERA5 and HadSLP2 is 0.92 ($P < 0.01$). Therefore, ERA5 reproduces the spatiotemporal distribution of MSLP over the research domain reasonably well.

The research domain mainly covers Mongolia, northern China, and southeastern Russia, with a complex terrain. The central and western parts of the research domain are the Mongolian Plateau, and the eastern part is the Northeast China plain. The most complex terrain is in Mongolia. The country occupies about 1.5 million square kilometers, has a mean elevation of 1580 m, and Khüiten Peak in the west

(‘upstream’) has the highest elevation 4374 m. Besides, there are many mountain ranges in the research domain, including the Altai Mountains, the Sayan Mountains, the Hangayn Mountains, the Stanovoy Upland, the Greater Khingan Mountains, and the Changbai Mountains. The terrain over the research domain refers to Fig. 1a. The boreal spring is referred to March–April–May (MAM), and the research period is 1979–2021 in this paper.

2.2 ETC detection and tracking algorithm

In this paper, the ETCs are objectively detected and tracked by the algorithm developed at the University of Melbourne by Murray and Simmonds (1991), Simmonds et al. (1999),

and Pezza et al. (2008), which captures both the pressure field and vorticity field characteristics of the ETCs (Hodges et al. 2003; Neu et al. 2013). The algorithm is performed as follows. First, the algorithm obtains the local minimum of the MSLP (minMSLP) and the local maximum of the Laplacian of the MSLP (maxLPslp) and then searches the minMSLP within 12 degrees around the maxLPslp. If a minMSLP is found, the ETC center is defined as the minMSLP; otherwise, the ETC center is defined as the point with the minimum MSLP gradient within 12 degrees around maxLPslp. Second, the algorithm tracks the ETC centers at time t and time $t + 1$ by steering the wind velocity and the last displacement of the ETC. More details can be found in Murray and Simmonds (1991) and Simmonds et al. (1999).

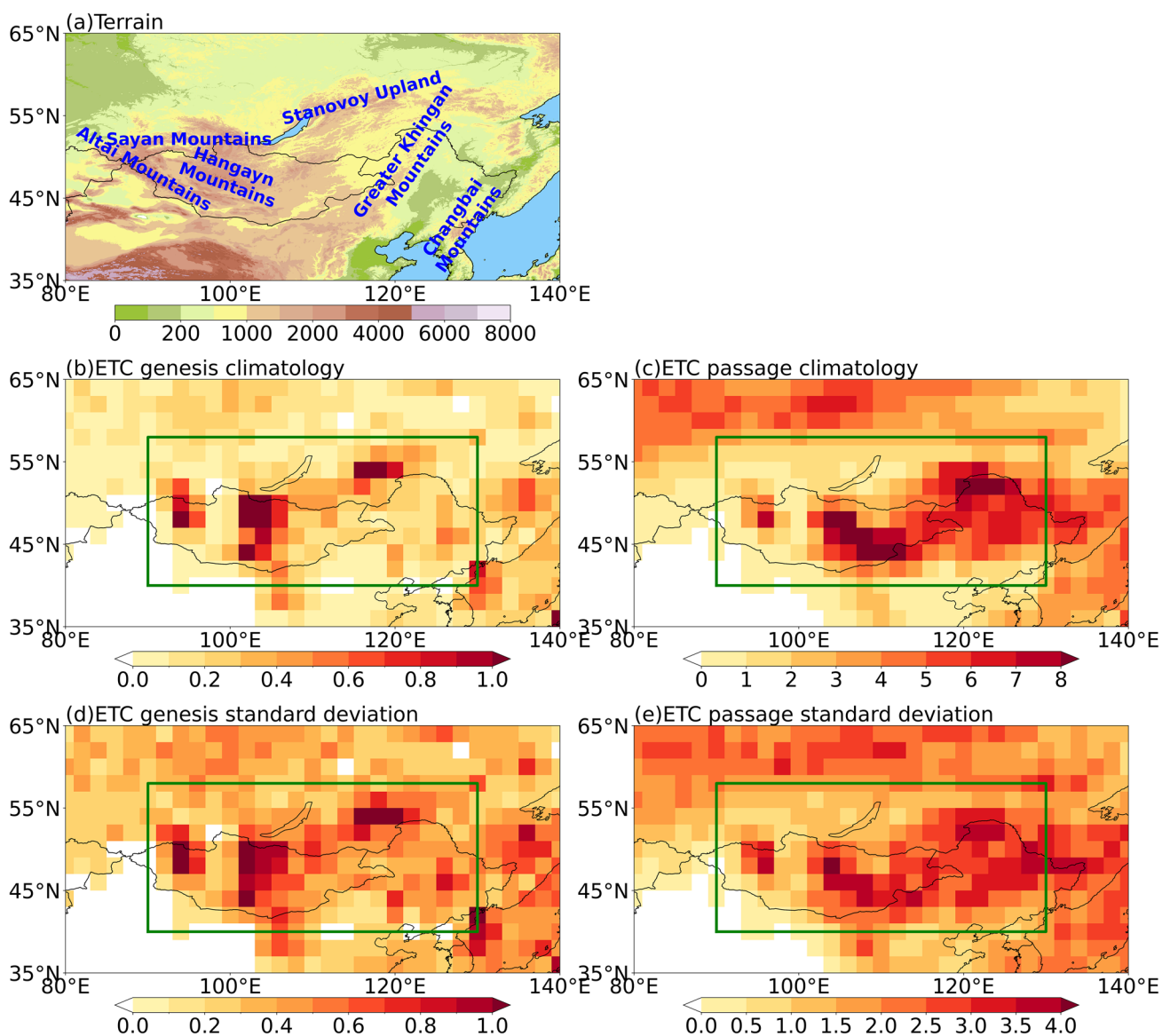


Fig. 1 a Terrain of the research domain (unit: m). Distributions of (b, c) climatology (unit: number spring⁻¹) and (d, e) standard deviation (unit: number spring⁻¹) of (b, d) ETC genesis and (c, e) ETC passage in spring during 1979–2021. The green box indicates the track selection domain

To remove the interference of seasonal and local thermal lows, we eliminate ETCs with lifetime less than 1 day (Wang et al. 2009; Zhang et al. 2012; Tamura and Sato 2022).

Previous studies have shown that MSLP still has physical meaning in characterizing ETCs over the Mongolian region, although MSLP is affected by high terrain. For example, Zhang et al. (2012) and Wu et al. (2022) compared manually identified ETCs with those identified using Melbourne University algorithm based on MSLP, and found good consistency between them. This may be attributed to the Melbourne University algorithm, which reduces terrain impact on MSLP by terrain correction parameter (Simmonds et al. 1999). Therefore, using MSLP to identify and track ETCs in this area is reasonable.

2.3 Definitions of ETC properties

The ETC genesis is defined as the first position of an ETC track. The ETC frequency is defined as the number of ETC tracks. ETC passage is defined as the number of ETCs passing through the grid point, and only the first time is counted if an ETC passes through the same grid point more than once.

The lifetime is defined as the time from the first point to the last point of an ETC track. For example, since we use 3-hourly resolution data, the lifetime is 24 h for an ETC track that includes 9 points. The moving distance is defined as the sum of the ETC distances at each adjacent time. The moving speed is defined as the moving distance of two adjacent times divided by the temporal resolution of 3-h. The average moving speed refers to the average moving speed in the entire lifetime of an ETC, and the maximum moving speed is defined as the maximum moving speed in the entire lifetime of an ETC. In addition, we use two metrics to investigate the variations in intensity. The two metrics are the central sea level pressure (Cslp) and Laplacian of sea level pressure (LPslp). The former is defined as the sea level pressure at the ETC center, and the latter is defined as the average LPslp within a 4-degree radius around the ETC center; for more details, refer to Simmonds et al. (1999) and Pinto et al. (2005).

2.4 ETC clustering

Nakamura et al. (2009) introduced a method to classify tropical cyclones based on mass moments. We adjust the method and apply it to the ETC classification. The details are as follows.

2.4.1 Standard deviation ellipse method

The standard deviation ellipse method can be used to measure the direction and distribution of a set of data (for example, an ETC track). The standard deviation ellipse calculated using a certain attribute value related to the feature as a weight is called the weighted standard deviation ellipse, which can be calculated according to the following formulas:

$$\bar{X} = \frac{1}{\sum_{i=1}^N w(i)} \sum_{i=1}^N w(i) * x(i) \quad (1)$$

$$\bar{Y} = \frac{1}{\sum_{i=1}^N w(i)} \sum_{i=1}^N w(i) * y(i) \quad (2)$$

$$Var(x) = \frac{1}{\sum_{i=1}^N w(i)} \sum_{i=1}^N w(i) * (x(i) - \bar{X})^2 \quad (3)$$

$$Var(y) = \frac{1}{\sum_{i=1}^N w(i)} \sum_{i=1}^N w(i) * (y(i) - \bar{Y})^2 \quad (4)$$

$$Var(xy) = \frac{1}{\sum_{i=1}^N w(i)} \sum_{i=1}^N w(i) * (x(i) - \bar{X}) * (y(i) - \bar{Y}) \quad (5)$$

where $x(i)$ and $y(i)$ are the longitude and latitude, respectively, of the ETC track at time i , $w(i)$ is the intensity of the ETC at the same time (the Cslp or LPslp is used here), and N is the number of ETC track positions. According to Formulas 6–11, the above five parameters can be transformed into an ellipse (\bar{X} , \bar{Y} , θ , σ_x and σ_y are the center, rotation angle, semimajor axis and semiminor axis of the ellipse, respectively), known as the weighted standard deviation ellipse.

$$A = Var(x) - Var(y) \quad (6)$$

$$B = \sqrt{(A^2 + C^2)} \quad (7)$$

$$C = 2 * Var(xy) \quad (8)$$

$$\theta = \tan^{-1}\left(\frac{A+B}{C}\right) \quad (9)$$

$$\sigma_x = \sqrt{2 * (Var(x) * \cos^2\theta + Var(y) * \sin^2\theta - 2 * Var(xy) * \sin\theta * \cos\theta)} \quad (10)$$

$$\sigma_y = \sqrt{2 * (Var(x) * \sin^2\theta + Var(y) * \cos^2\theta - 2 * Var(xy) * \cos\theta * \sin\theta)} \quad (11)$$

The five variables to the left of the equal sign in Formulas 1–5 represent the center longitude, center latitude, zonal variance, meridional variance, and diagonal variance of the ETC track, including the information of the track center position, track length, and track direction. This method can convert ETC tracks of different points into 5 parameters, facilitating the application of K-means clustering. Therefore, we use these five parameters to cluster the ETCs.

2.4.2 K-means clustering

The K-means clustering algorithm is a commonly used iterative unsupervised clustering algorithm (Catto 2018; Nie and Sun 2022). The main idea is to divide the given sample set into K clusters so that the similarity of points within the clusters is as high as possible and the similarity between different clusters is as low as possible, thereby clustering a given dataset into K categories. Distance is usually used as a similarity indicator. Each cluster is described by a cluster center, which is calculated from the mean of all values in the cluster.

In this paper, the Calinski–Harabasz score (Caliński and Harabasz 1974) is used to obtain the optimal number of clusters. The Calinski–Harabasz score, also known as the Variance Ratio Criterion, is defined as the ratio of the sum of between-cluster dispersion and the sum of within-cluster dispersion for all clusters (where dispersion is defined as the sum of distances squared). Generally, a higher score indicates better clustering performance.

2.5 Statistical test

The moving t-test is used to identify the significant abrupt change year in the time series. The Mann–Whitney *U* test (Mann and Whitney 1947) is used to test whether two samples of data were from the same distribution.

3 Characteristics of Mongolian ETCs

3.1 Climatology and trends of Mongolian ETC frequency

Climatological features of ETCs over the Mongolian region in spring during 1979–2021 are presented in Fig. 1b–e. There are three major areas of ETC genesis, located in downstream regions of the Altai-Sayan Mountains, the Hangayn Mountains and the Stanovoy Upland (Fig. 1b). Northeast China, Southeast Russia, the downstream region

of the Changbai Mountains, and the region to the northwest of Lake Baikal are the submajor areas of ETC genesis. This distribution pattern is closely related to the local terrain. The dynamic action corresponding to the leeward slope area (e.g., the downstream regions of the Altai-Sayan Mountains and the Hangayn Mountains) is conducive to ETC genesis, which is so-called lee genesis (Chung et al. 1976; Adachi and Kimura 2007; Lee et al. 2020). The distribution of the standard deviation of ETC genesis (Fig. 1d) is similar to its climatology, with high values in the Altai-Sayan Mountains, the Hangayn Mountains, the Stanovoy Upland, and the Greater Khingan Mountains. The climatological ETC passage, as shown in Fig. 1c, is pronounced in a zonal area from central Mongolia to Northeast China. The distribution of the standard deviation of the ETC passage also resembles its climatology. The above distributions are similar to those of previous studies (Adachi and Kimura 2007; Wang et al. 2009; Zhang et al. 2012; Fu et al. 2013; Lee et al. 2020) but provide more detailed information because the spatial and temporal resolution of the data used in this study is higher. For example, previous studies have captured only one genesis center in the downstream region of the Altai-Sayan Mountains, while genesis centers near the Stanovoy Upland and the Greater Khingan Mountains are captured here. In addition, the ETC genesis and passage here are also greater than those in previous studies because of higher spatial and temporal resolution.

Based on Fig. 1b–e, we chose 40°–58°N, 90°–130°E (green box in Fig. 1) as the research domain, and ETCs lasting more than 1 day in the domain are retained. According to the ETC formed in the domain or that entered the domain, we divide the ETCs into two categories, named “Formed ETCs” and “Entered ETCs”, and the sum of the two types is named “All ETCs”. As shown in Fig. 2, the genesis location of the Formed ETCs (dark red points in Fig. 2a) is consistent with the ETC genesis distribution in Fig. 1b. Most of the Formed ETCs move eastward. Finally, these ETCs decay in East Siberia, North China, the Sea of Japan and the Northwest Pacific. Entered ETCs are generated in Siberia and the Loess Plateau; these ETCs enter the research domain from the west, north and south (Fig. 2b) and ultimately decay in Mongolia, Northeast China and the Northwest Pacific.

Moreover, the Formed ETCs (37.1 cyclones per year on average) account for the majority of All ETCs (40.1 cyclones per year on average) compared with the Entered ETCs (3.0 cyclones per year on average) (Fig. 2c–e). In addition, the correlation coefficient between the frequency time series of the Formed ETCs and All ETCs is 0.97 ($P < 0.01$). These

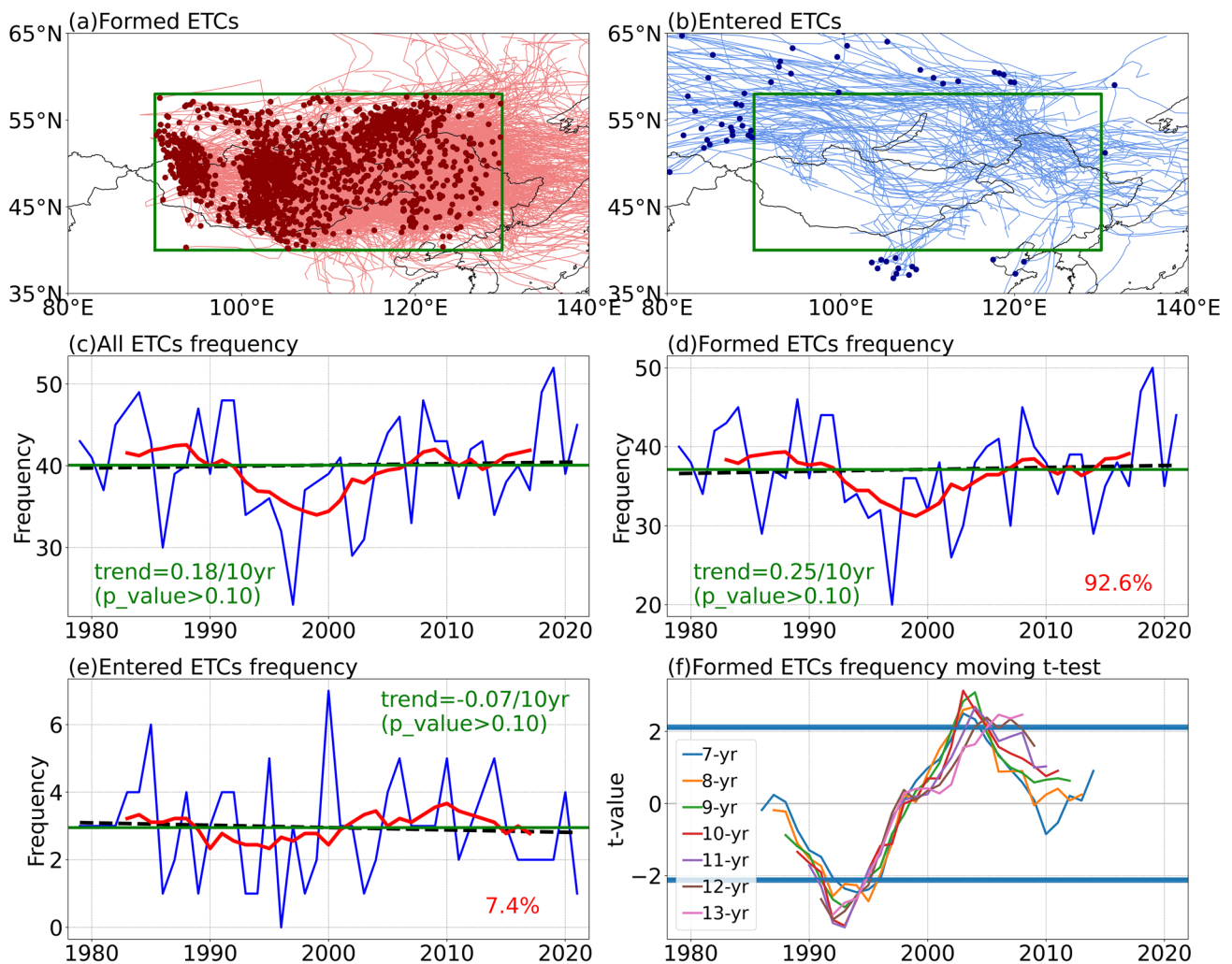


Fig. 2 Distributions of (a) Formed (red) and (b) Entered (blue) ETCs genesis locations (solid points) and tracks (solid lines). Time series of (c) All, (d) Formed and (e) Entered ETCs frequency (unit: number spring⁻¹) over Mongolia in spring during 1979–2021. (f) Moving t-test of series in (d) with windows of 7–13 years. The green boxes in

(a, b) indicate the track selection domain. The solid blue lines, solid red lines, dashed black lines and solid green lines in (c–e) are the original sequences, 9-year moving averages, linear trends and means of ETC frequency, respectively. The horizontal solid lines in (f) indicate the 0.05 significance level

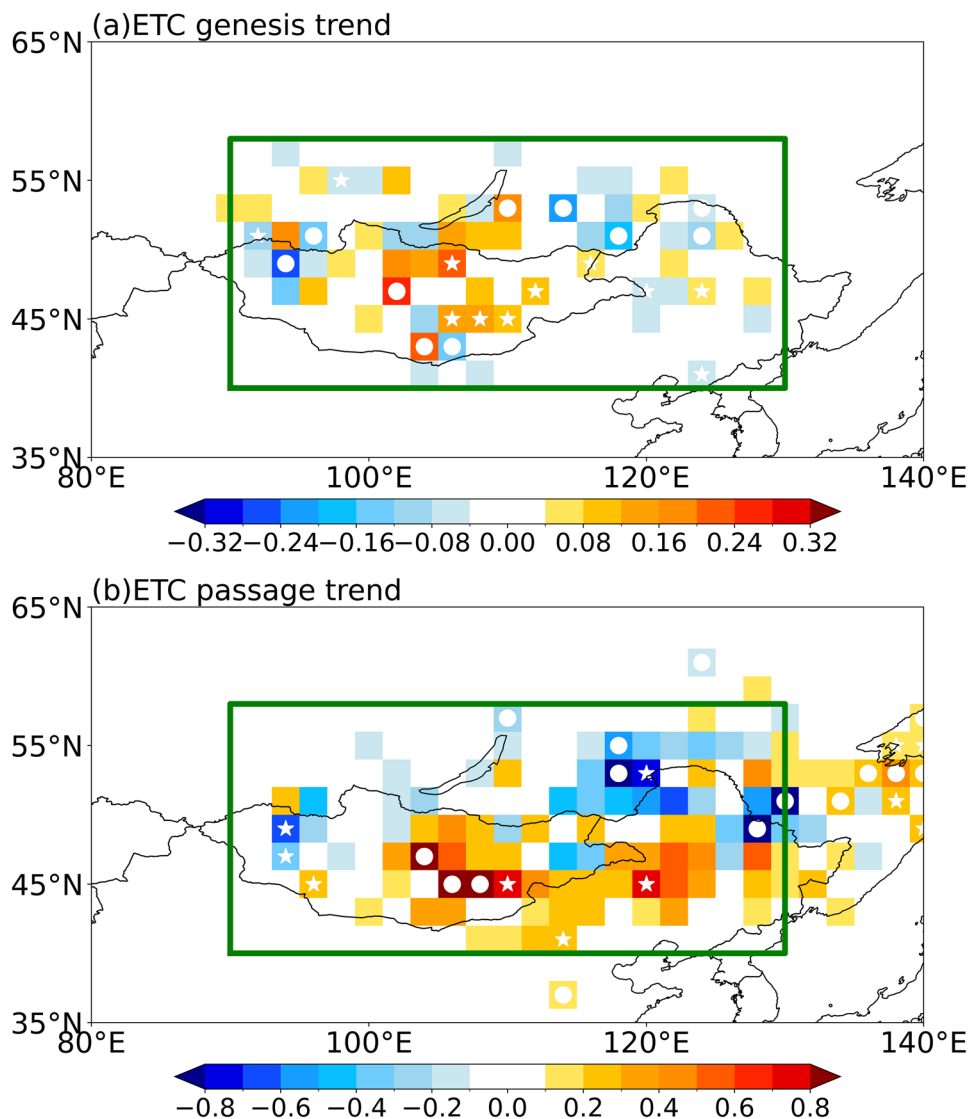
results indicate that the ETCs over the Mongolian region are mainly locally generated. Thus, we focus on the Formed ETCs in the following sections and call them the “Mongolian ETCs”.

Although the time series of Mongolian ETCs show no significant trend during 1979–2021 (Fig. 2d), significant interdecadal changes can be found in approximately 1993 and 2004 (Fig. 2f, $P < 0.05$) based on moving t-test. The mean frequencies during 1979–1992, 1993–2003 and 2004–2021 are 39.4, 31.6 and 38.7, respectively, presenting a “high–low–high” variation. This variation is consistent with previous studies (Huang et al. 2016), but the frequency is greater than that in previous studies (Wang et al. 2009; Huang et al. 2016), because of the higher spatiotemporal resolution of the reanalysis dataset used in this study. In

addition, our analysis reveals that there are more ETCs in recent years, for example, 2018 and 2019 are the two years with the highest ETC frequency in the past 43 years.

In addition to the temporal changes, the spatial distributions of the genesis and passage trends of Mongolian ETCs are also investigated. ETC genesis increases significantly around central Mongolia but decreases in western Mongolia and to the east of Lake Baikal (Fig. 3a). Moreover, the ETC passage increases significantly from central Mongolia to Northeast China but decreases in western Mongolia and to the east of Lake Baikal (Fig. 3b). Such a “south positive–north negative” trend pattern indicates that the tracks of Mongolian ETCs tend to move southward.

Fig. 3 Linear trends (unit: number spring⁻¹ decade⁻¹) of (a) ETC genesis and (b) ETC passage in spring during 1979–2021. The green box indicates the track selection domain. White dots and pentagrams indicate regions over which the trends are significant at $P < 0.05$ and $P < 0.10$, respectively



3.2 Characteristics of Mongolian ETC lifetime, moving distance, moving speed and intensity

In addition to the ETC frequency, other properties of the ETC, such as lifetime, moving distance, moving speed, and intensity, are also very important. The characteristics of the probability density function (PDF) of Mongolian ETC properties are first investigated (Fig. 4). The lifetime PDF (Fig. 4a) is similar to an exponential distribution, and the PDFs of the other properties (moving distance, average speed, maximum speed, average Cslp, minimum Cslp, average LPslp and maximum LPslp, Fig. 4b–h) are similar to a skewed distribution, and they are all right skewed distributions.

Specifically, the ETC frequency decreases with increasing of lifetime. Approximately 50% of cyclones last 1.75 days (42.0 h) or less, the average lifetime is 2.23 days (53.5 h), the maximum lifetime is 11.50 days (276.0 h), and the minimum

lifetime is 1.00 days (24.0 h) according to the definition. The distribution of the moving distance is positively skewed, the ETC frequency is the highest near 1200 km, and approximately 50% of cyclones move 1628 km or less. The minimum, average and maximum distances are 233 km, 1900 km and 11,323 km, respectively. The distribution of the average speed is closer to the normal distribution, and the minimum, average and maximum are 7.03 km h⁻¹, 37.34 km h⁻¹ and 94.64 km h⁻¹, respectively. The distribution of the maximum speed is similar to that of the moving distance, with minimum, average and maximum values of 14.71 km h⁻¹, 94.11 km h⁻¹ and 281.57 km h⁻¹, respectively. The PDFs of the average and minimum Cslp are both similar to the normal distribution, with averages of 1004 hPa and 999 hPa, respectively. However, the PDFs of the average and maximum LPslp are both positively skewed, with averages of 0.91 hPa deg.lat.⁻² (the unit refer to Simmonds et al. (1999)) and 1.50 hPa deg.lat.⁻², respectively.

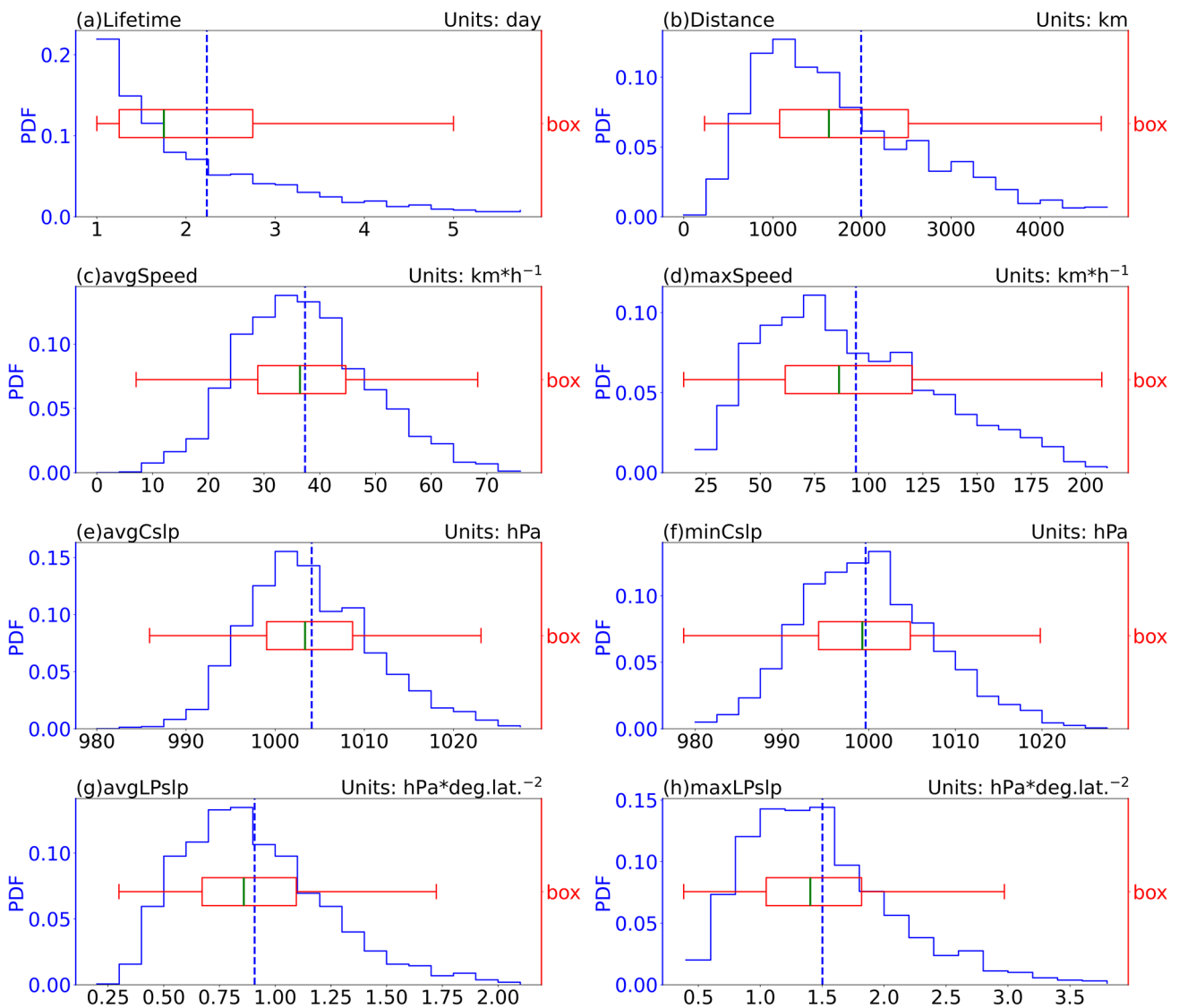


Fig. 4 Probability density function (blue) and boxplot (red) of (a) lifetime (unit: day), (b) distance (unit: km), (c) average speed (unit: km h^{-1}), (d) maximum speed (unit: km h^{-1}), (e) average Cslp (unit: hPa), (f) minimum Cslp (unit: hPa), (g) average LPslp (unit: $\text{hPa deg. lat.}^{-2}$)

and (h) maximum LPslp (unit: $\text{hPa deg. lat.}^{-2}$) for Mongolian ETCs in spring during 1979–2021. The vertical dashed lines indicate the means

The aforementioned Mongolian ETC properties also show strong variability (Fig. 5). The average lifetime slightly increases by 0.01 days (0.34 h) per decade (not significant), and the average distance increases by 47.2 km per decade ($P < 0.10$). In addition to the linear trend, the average lifetime and average distance exhibit decadal changes in the early 1990s (Fig. 5a, b). Besides, there is a high correlation between the two properties, with a coefficient of 0.88 ($P < 0.01$). The average speed significantly increases during 1979–2021, with a trend of 0.80 km h^{-1} per decade ($P < 0.01$). Furthermore, the average speed also shows a decadal increase in the 1990s (Fig. 5c). The maximum speed of

Mongolian ETCs also shows a strong increasing trend in the last four decades (Fig. 5d; 1.90 km h^{-1} per decade, $P < 0.05$). The ETC intensity indices show significant trends and inter-decadal variations. The average Cslp and minimum Cslp present similar changes (Fig. 5e, f). The average Cslp significantly decreases during 1979–2021, with a linear trend of -0.44 hPa per decade ($P < 0.05$), and the minimum Cslp shows a trend of -0.52 hPa per decade ($P < 0.05$). Notably, there are significant decadal decreases in average Cslp and minimum Cslp in the mid-1990s.

Our other intensity metric also shows consistent signals (Fig. 5g, h). The average LPslp shows a strong positive

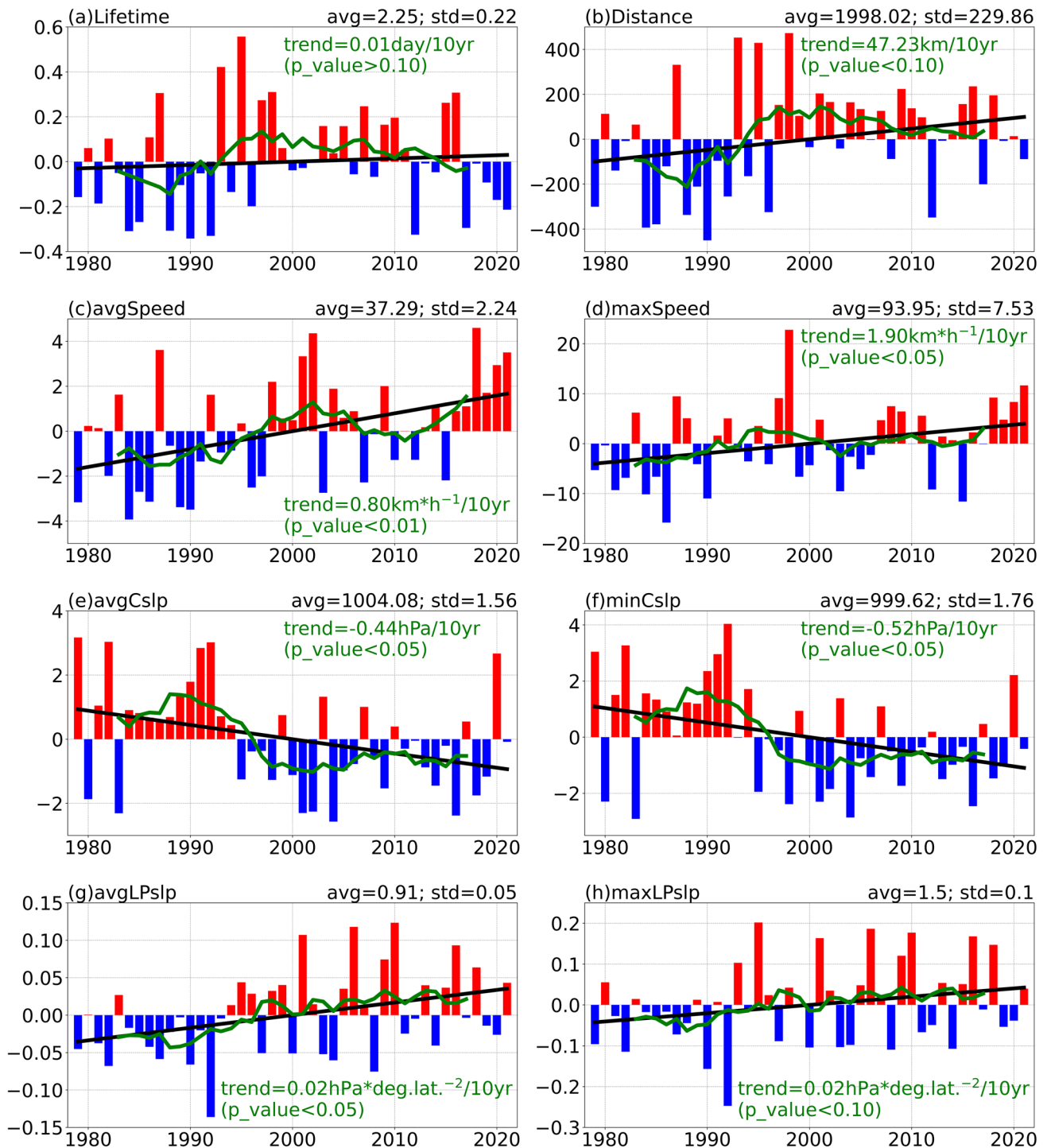


Fig. 5 Time series of (a) lifetime (unit: day), (b) distance (unit: km), (c) average speed (unit: km h^{-1}), (d) maximum speed (unit: km h^{-1}), (e) average Cslp (unit: hPa), (f) minimum Cslp (unit: hPa), (g) average LPslp (unit: hPa deg.lat.^{-2}) and (h) maximum LPslp (unit: hPa deg.lat.^{-2}) anomalies for Mongolian ETCs in spring during 1979–2021. The bar, green line and black line are the anomaly sequence, 9-year moving average and linear trend, respectively. The trend and *P*-value of the sequence are marked in green font in each panel

trend of $0.02 \text{ hPa deg.lat.}^{-2}$ per decade ($P < 0.05$), and the maximum LPslp presents a trend of $0.02 \text{ hPa deg.lat.}^{-2}$ per decade ($P < 0.10$). The average LPslp and maximum LPslp

also undergo decadal increases in the mid-1990s. The above results unanimously indicate that Mongolian ETCs have significantly strengthened over the past 43 years.

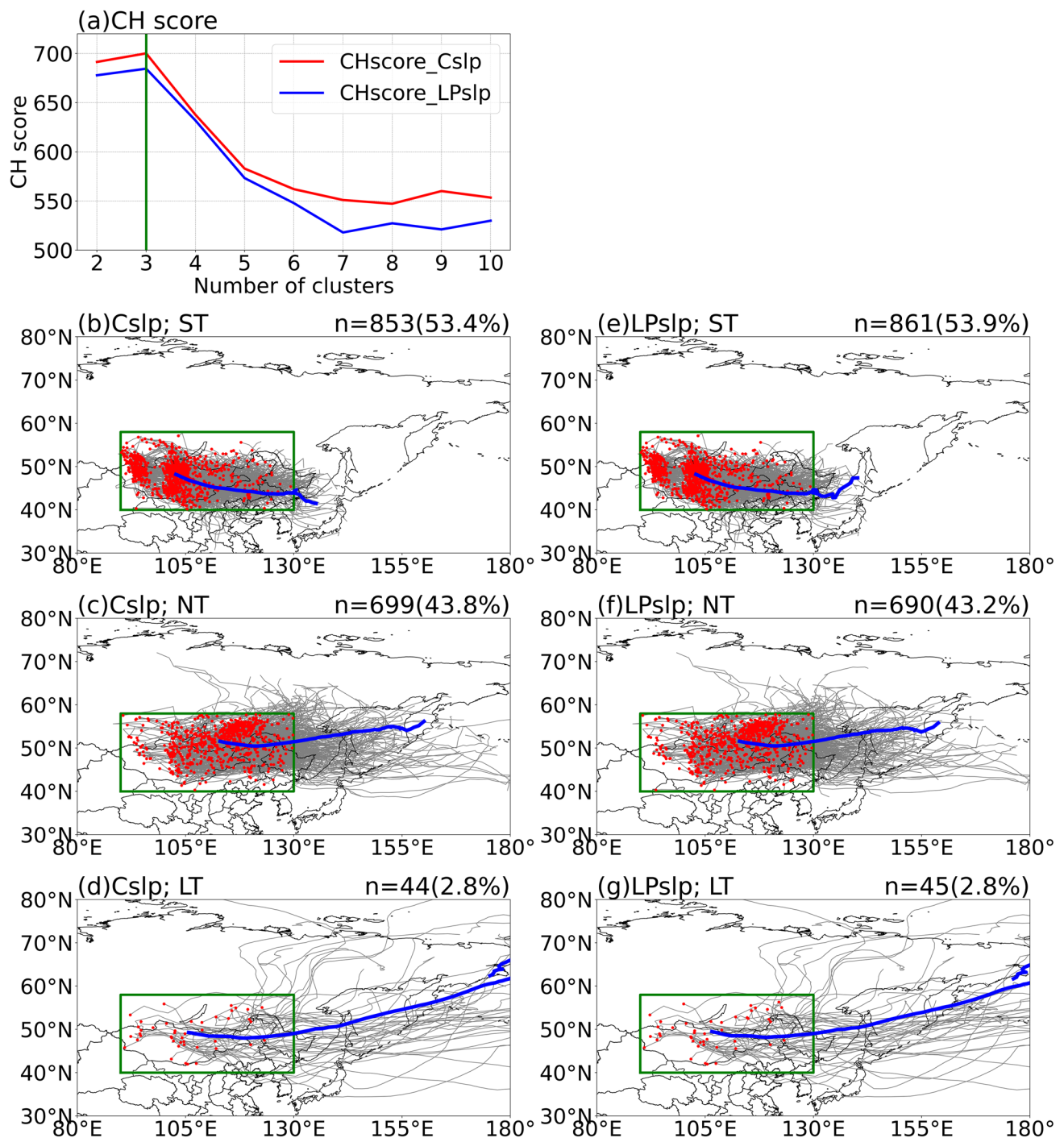


Fig. 6 a Calinski–Harabasz score corresponding to different cluster numbers based on Cslp (red line) and LPslp (blue line) weights. **b–d** ETC genesis locations (red points) and tracks (gray lines) clustered

into three categories based on Cslp weights. **e–g** As in **(b–d)**, but for the LPslp weights. The blue lines in **(b–g)** indicate the mean track, and the green boxes in **(b–g)** indicate the track selection domain

4 Clustering of Mongolian ETCs and characteristics of different clusters

4.1 Clustering of Mongolian ETCs

In this section, the clustering method is used to study the regional features of Mongolian ETCs. The ETC tracks are first transformed into a dataset of five parameters based on the standard deviation ellipse method, making it possible to classify all the ETC tracks. Then, K-means clustering is used for analysis. The Calinski–Harabasz score indicates that the best number of clusters is 3 (Fig. 6a), implying that there are three categories of Mongolian ETCs. The tracks of the three categories of Mongolian ETCs based on the Cslp and LPslp weights are shown in Fig. 6b–d and e–g, respectively. Taking the results based on the Cslp weights as an example, the three categories of Mongolian ETCs have different characteristics. There are 853 ETC tracks in Cluster 1 (Fig. 6b), accounting for 53.4% of the total number of Mongolian ETC tracks. These ETCs mostly generate in central and western Mongolia, and then move eastward along a southern path, passing through Mongolia, Inner Mongolia and southern Northeast China. Therefore, the ETCs in Cluster 1 are named southern track (ST) ETCs.

There are 699 ETC tracks in Cluster 2 (Fig. 6c), accounting for 43.8% of the total number of Mongolian ETC tracks. These ETCs mostly generate in central and eastern Mongolia and to the east of Lake Baikal, and then move eastward along a northern path, passing through Mongolia, Siberia, Inner Mongolia and northern Northeast China. Therefore, this type of ETC is named northern track (NT) ETCs. Cluster 3 has the smallest number of ETC tracks, accounting for approximately 2.8% of the total number of Mongolian ETCs. The ETC tracks in this cluster have longer moving distances, which suggests that the ETCs in Cluster 3 could had a stronger intensity and destructive power. Therefore, this type of ETC should be also studied, although its number is much less than that of the other two clusters. Based on the long distance characteristics, the ETCs in Cluster 3 are named long track (LT) ETCs.

The results based on the LPslp weights (Fig. 6e–g) are similar to those based on the Cslp weights (Fig. 6b–d), and the numbers (proportions) of ST, NT, and LT ETCs are 861 (53.9%), 690 (43.2%), and 45 (2.8%), respectively. The consistency of the results based on different weight metrics further verifies the rationality of the aforementioned ETC classification.

According to Fig. 6, there are differences in the genesis locations of the three categories of ETCs. To further confirm this speculation, the probability density functions (PDFs) for the genesis longitude and latitude of the three categories of ETCs are displayed in Fig. 7. Based on the Cslp weights, the

average genesis locations (longitudes, latitudes) for the ST, NT, and LT ETCs are (102.8°E, 48.2°N), (113.0°E, 51.5°N), and (105.7°E, 49.3°N), respectively. The differences among the ST, NT, and LT genesis longitudes (latitudes) are significant ($P < 0.05$ for longitudes and $P < 0.10$ for latitudes) based on the Mann–Whitney U test. The results based on the LPslp weights are consistent (Fig. 7d, f): the average genesis locations for the ST, NT, and LT ETCs are (102.9°E, 48.2°N), (112.9°E, 51.6°N), and (106.5°E, 49.5°N), respectively. The above results further confirm the rationality of dividing Mongolian ETCs into three categories (ST, NT and LT ETCs). For convenience, the clustering results based on the Cslp weights will be used in the following analysis.

The distributions of ETC genesis and passage in the three clusters are shown in Fig. 8. The figure suggests that areas with a high genesis frequency for ST ETCs are located mainly in central and western Mongolia (Fig. 8a), and that for NT ETCs are located mainly to the east of Lake Baikal (Fig. 8b), which are consistent with the two major activity centers of the Mongolian ETCs (Fig. 1b). Moreover, the passages of the ST and NT ETCs (Fig. 8d–e) also exhibits features similar to those of the Mongolian ETCs (Fig. 1c). Due to the small number of LT ETCs, their contribution to the Mongolian ETCs is also limited (Fig. 8c, f).

The trends in the frequency of genesis and passage of the ST, NT and LT ETCs are depicted in Fig. 8g–l. The frequency of ST ETCs genesis shows a significant positive trend near central Mongolia (Fig. 8g), and there is a significant positive trend of ETC passage in the zonal region from central Mongolia to southern Northeast China (Fig. 8j). The frequency of NT ETCs genesis shows a negative trend to the east of Lake Baikal (Fig. 8h), and there is a significant negative trend of NT passage in the zonal region from Lake Baikal to northern Northeast China (Fig. 8k), which are consistent with the aforementioned “south positive-north negative” trend pattern of the Mongolian ETCs in Fig. 3.

The temporal variation characteristics of the ST, NT and LT ETCs are further analyzed (Fig. 9). For convenience, the results based on the Cslp weights are taken as an example in the following analysis. The ST ETCs has a significant increasing trend (Fig. 9a; 0.97 per decade, $P < 0.10$). The recent increase in ST ETCs indicates that the impact of ST ETCs on the passing areas will be more noticeable, which may not be explained by all the Mongolian ETCs. In contrast, the NT ETCs has a significant decreasing trend (Fig. 9b; -0.82 per decade, $P < 0.10$). Therefore, increasing Mongolian ETCs are mainly contributed by ST ETCs in recent years. The opposite frequency trends of the ST and NT ETCs are consistent with the opposite spatial trends of genesis and passage shown in Fig. 8. In addition, the ST and NT ETCs also undergo interdecadal changes, with shifts occurring in approximately 2004 and 1993 (Fig. 9d, e;

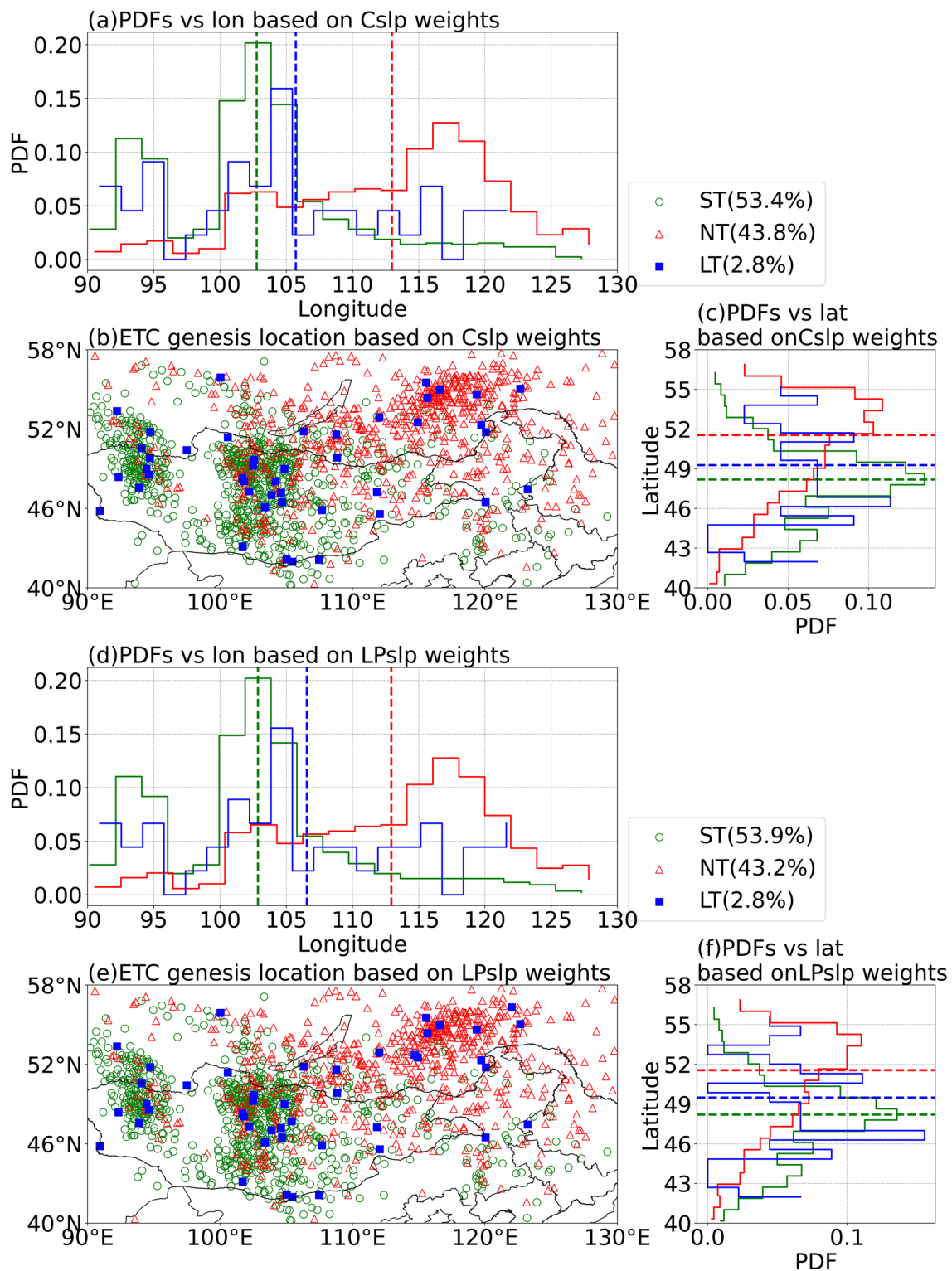


Fig. 7 ETC genesis (a) longitude, (b) location and (c) latitude distributions of ST ETCs (green), NT ETCs (red) and LT ETCs (blue) based on Cslp weights. (d–f) As in (a–c), but for the LPslp weights. The dashed lines in (a, c, d, f) represent the means

$P < 0.05$), respectively. On the one hand, because the trends of the ST and NT ETCs are opposite, the Mongolian ETCs show no significant trend over the past 43 years (Fig. 2d). On

the other hand, the ST and NT ETCs contribute to the two decadal changes in the Mongolian ETCs in approximately 2004 and 1993, respectively (Figs. 9d, e and 2f). Conversely,

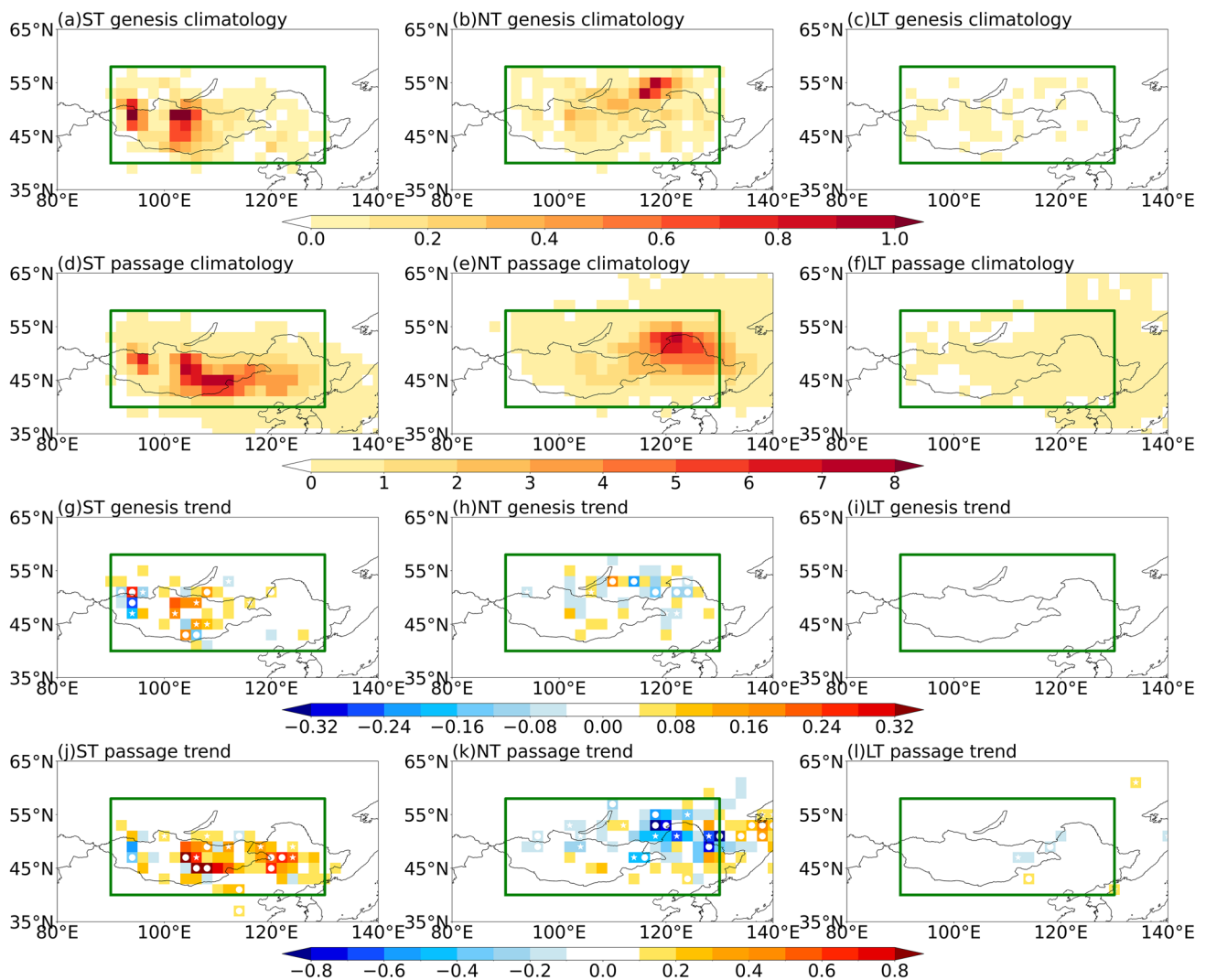


Fig. 8 Distributions of climatology (unit: number spring⁻¹) for (a–c) genesis and (d–f) passage in spring during 1979–2021. Linear trend (unit: number spring⁻¹ decade⁻¹) of (g–i) genesis and (j–l) passage in spring during 1979–2021. (a, d, g, j) for ST ETCs, (b, e, h, k) for NT

ETCs, and (c, f, i, l) for LT ETCs. The green box indicates the track selection domain. The white dots and pentagrams in (g–l) indicate regions over which the trends are significant at $P < 0.05$ and $P < 0.10$, respectively

LT ETCs have a small contribution to Mongolian ETCs due to their limited number.

4.2 Characteristics of lifetime, moving distance, moving speed and intensity for different clusters

After understanding the characteristics of the ST, NT and LT frequencies, the PDFs of the ST, NT and LT ETC properties are shown in Fig. 10. The PDF distributions of ST and NT ETCs are generally similar to the distributions of Mongolian ETCs (Fig. 4), but the distributions of LT ETCs are significantly different. Specifically, ST ETCs are mainly distributed in short-lifetime region, NT ETCs have a higher frequency in long-lifetime region, and LT ETCs have a lifetime of more

than 4 days (Fig. 10a). Correspondingly, the ST ETCs are mainly concentrated in short-distance regions, and the NT ETCs are located much longer distances, and the distances of LT ETCs are mostly greater than 5000 km (Fig. 10b). The above results indicate that the left side of Fig. 4a, b is mainly contributed by ST ETCs, the right side is mainly contributed by ST ETCs, and the right tail region is mainly contributed by LT ETCs. For the average speed, NT ETCs are the slowest, ST ETCs are faster, and LT ETCs are the fastest (Fig. 10c). There is no obvious difference between the PDFs of maximum speeds for the ST and NT ETCs, but the maximum speeds of the LT ETCs are significantly faster than those of the other two ETCs (Fig. 10d). The intensity distributions of the three categories of ETCs (Fig. 10e–h) indicate that LT ETCs are the strongest, NT ETCs are the

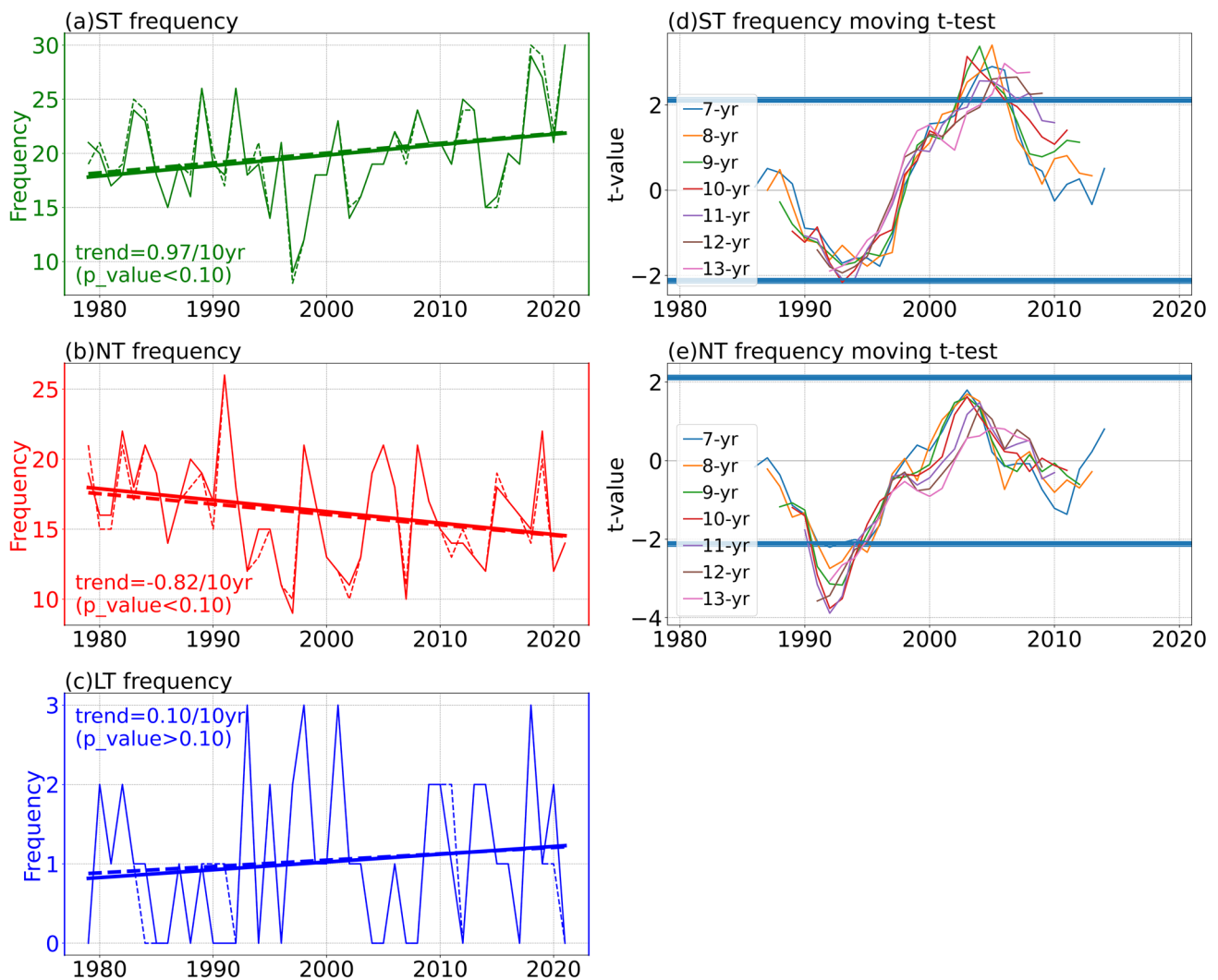


Fig. 9 Time series of (a) ST, (b) NT and (c) LT ETC frequency (thin solid line and thin dashed line; unit: number spring⁻¹) during 1979–2021. **d** Moving t-test of series in (a) with windows of 7–13 years. **e** As in (d), but for the series in (b). The thick lines in (a–c) indicate the

linear trends, and the solid (dashed) lines indicate the series based on Cslp (LPslp) weights. The horizontal solid lines in (d–e) indicate the 0.05 significance level. The trends and *P*-values of the sequences in (a, b, c) are marked in each panel

second, and ST ETCs are the least. Except for the nonsignificant difference in maximum speed between ST and NT ETCs, there are significant differences in other properties among the three categories of ETCs ($P < 0.01$ based on the Mann–Whitney *U* test).

Due to the limited number of LT ETCs, we analyze only the variability in the properties of the ST (Fig. 11) and NT ETCs (Fig. 12). The average lifetime of ST ETCs mainly manifests interannual and interdecadal variability but with no significant trend; in contrast, the average lifetime of the NT ETCs slightly increases (0.04 days per decade, not significant). The average distance of the ST ETCs exhibits interdecadal variability. In contrast, the average distance of NT ETCs significantly increases

(81.3 km per decade, $P < 0.05$), making a major contribution to the increase in Mongolian ETCs (Fig. 5b). The average speed and maximum speed of the ST ETCs show a slight increase. However, the average speed and maximum speed of NT ETCs show significant positive trends (1.1 km h⁻¹ per decade at $P < 0.01$ and 2.6 km h⁻¹ per decade at $P < 0.10$, respectively), favoring an increase in Mongolian ETCs (Fig. 5c, d). The average Cslp and the minimum Cslp of ST ETCs show interdecadal decreases during the mid-1990s, and the minimum Cslp shows significant negative trend (−0.42 hPa per decade, $P < 0.10$). Besides, the average Cslp and minimum Cslp of NT ETCs show significant decreasing trends (−0.64 hPa per decade at $P < 0.05$ and −0.69 hPa per decade at $P < 0.05$,

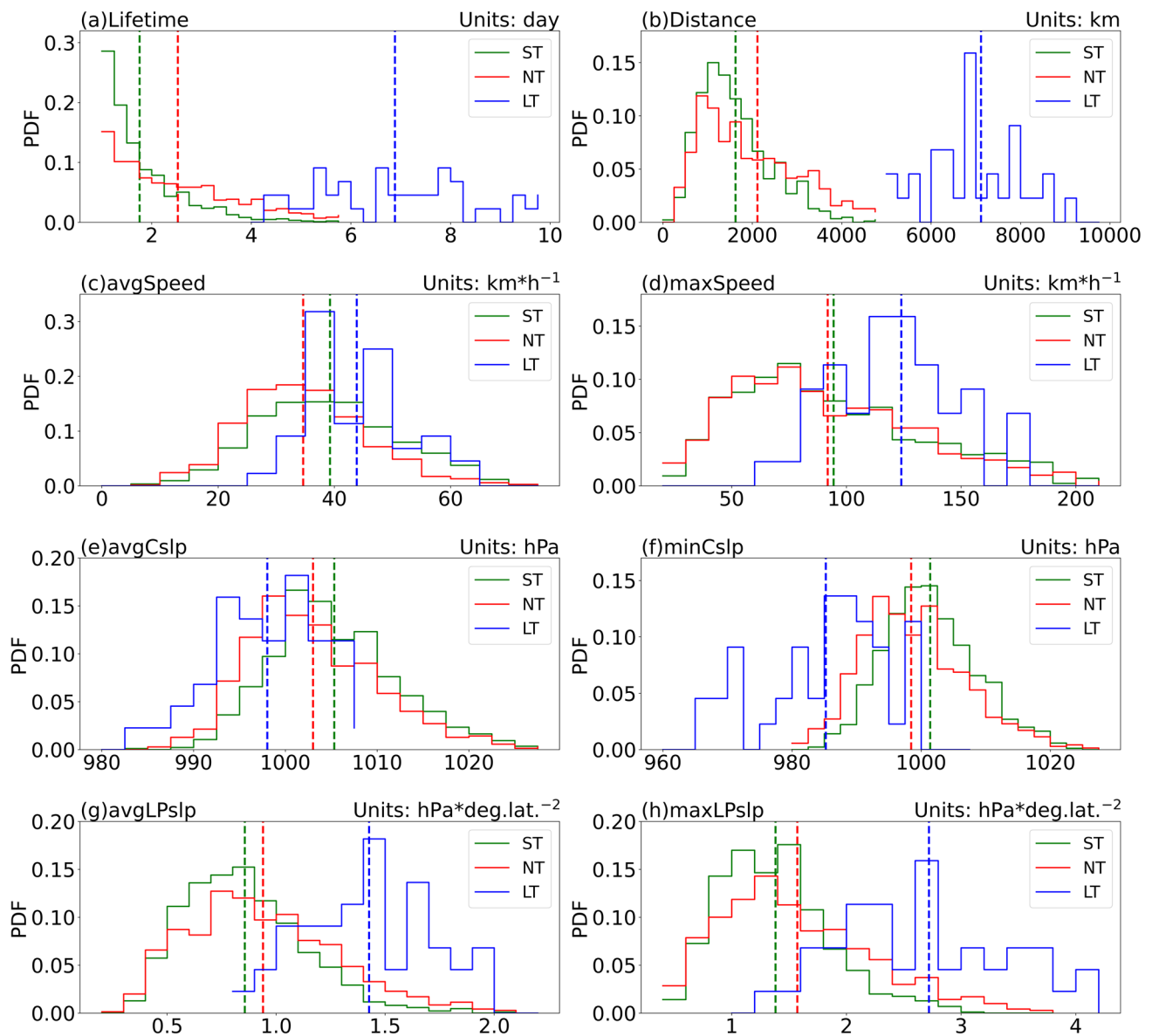


Fig. 10 Probability density functions of **(a)** lifetime (unit: day), **(b)** distance (unit: km), **(c)** average speed (unit: km h^{-1}), **(d)** maximum speed (unit: km h^{-1}), **(e)** average Cslp (unit: hPa), **(f)** minimum Cslp (unit: hPa), **(g)** average LPslp (unit: hPa deg.lat.^{-2}) and **(h)** maximum LPslp

(unit: hPa deg.lat.^{-2}) for ST ETCs (green), NT ETCs (red) and LT ETCs (blue) in spring during 1979–2021. The vertical dashed lines indicate the means

respectively). Therefore, the reductions in Cslp in both ST and NT ETCs contribute to the increase in the intensity of Mongolian ETCs (Fig. 5e, f). Moreover, due to the greater proportion of ST ETCs after the mid-1990s (Figs. 9a, b and 2d), their contribution to the enhancement of Mongolian ETCs is greater.

Another intensity indicator (i.e., LPslp) shows similar results. The average LPslp of the ST ETCs significantly increases ($0.01 \text{ hPa deg.lat.}^{-2}$ per decade, $P < 0.10$), and the average LPslp of the NT ETCs also significantly increases ($0.02 \text{ hPa deg.lat.}^{-2}$ per decade, $P < 0.05$).

Therefore, both of ST and NT ETCs are conducive to an increase in the average LPslp of Mongolian ETCs (Fig. 5g).

5 Discussion and conclusion

In this study, ETCs over the Mongolian region in spring during 1979–2021 are detected and tracked based on the ERA5 dataset (0.25-degree in spatial resolution and 3-hourly in temporal resolution). The characteristics

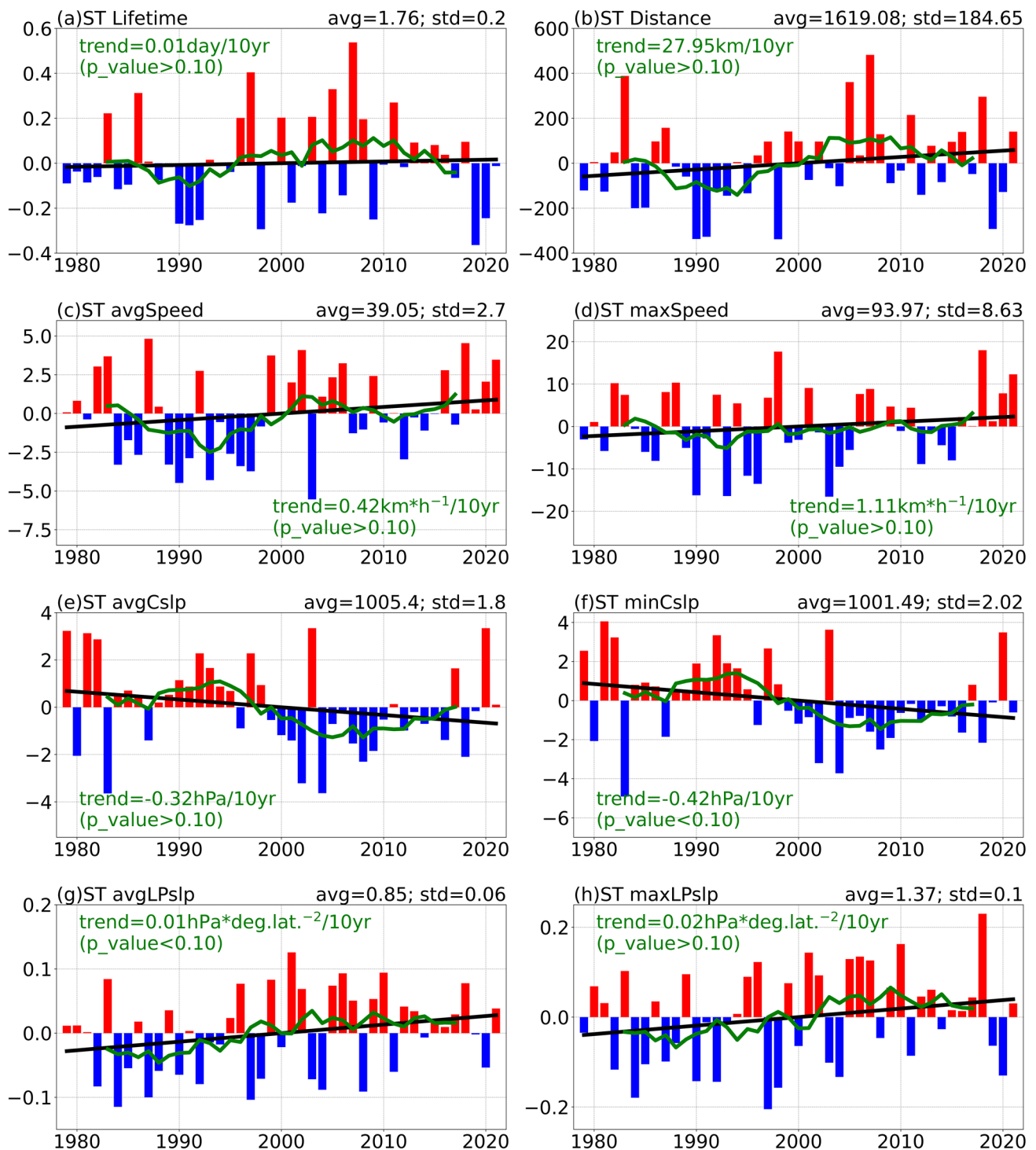


Fig. 11 Time series of **(a)** lifetime (unit: day), **(b)** distance (unit: km), **(c)** average speed (unit: km h^{-1}), **(d)** maximum speed (unit: km h^{-1}), **(e)** average Cslp (unit: hPa), **(f)** minimum Cslp (unit: hPa), **(g)** average LPslp (unit: hPa deg.lat.^{-2}) and **(h)** maximum LPslp (unit: hPa deg.lat.^{-2})

anomalies for ST ETCs in spring during 1979–2021. The bar, green line and black line are the anomaly sequence, 9-year moving average and linear trend, respectively. The trend and *P*-value of the sequence are marked in green font in each panel

of the genesis and passage of the above ETCs are examined, and then, Mongolian ETCs are selected. The characteristics of Mongolian ETC properties, including

lifetime, moving distance, moving speed and intensity, are further investigated. In addition, Mongolian ETCs are classified using the standard deviation ellipse method and

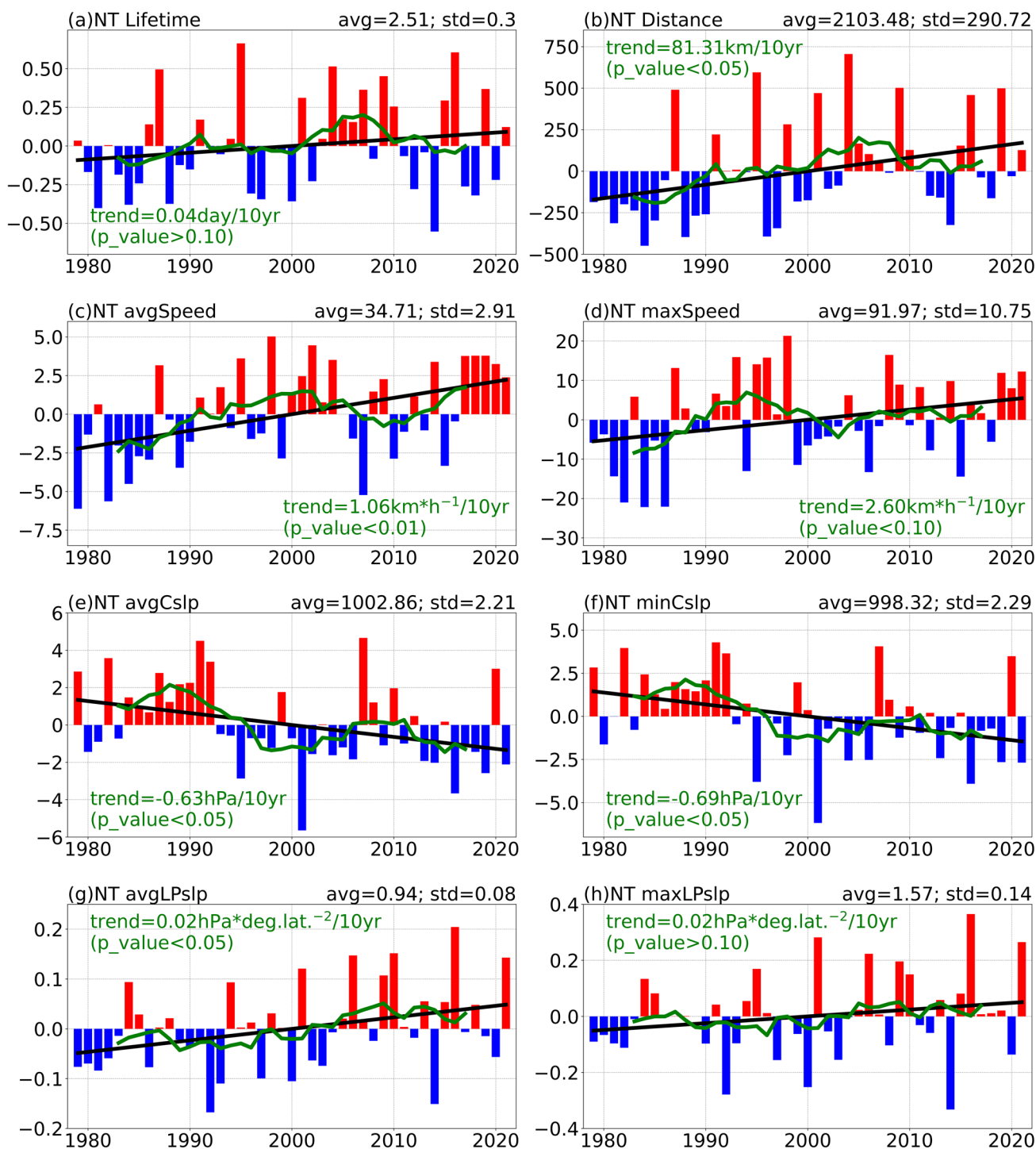


Fig. 12 As in Fig. 11, but for the NT ETCs

the K-means clustering method, and the characteristics of the classified ETC properties are further analyzed.

The results indicate that ETCs over the Mongolian region are mainly generated on the leeward slopes of the Altay-Sayan Mountains, Hangayn Mountains, Stanovoy Upland, and Greater Khingan Mountains. The area with a

high frequency of ETC passage is located in a zonal area from Mongolia to Northeast China. The standard deviation distributions of ETC genesis and ETC passage are similar to their climatology. In addition, there are two types of ETCs over Mongolia, i.e., Formed ETCs and Entered ETCs, accounting for 92.6% and 7.4%, respectively.

Therefore, the locally formed ETCs dominate and represent the major characteristics of ETCs over Mongolia. Although there is no significant trend in Mongolian ETC frequency, there are two decadal changes in approximately 1993 and 2004, showing a “high–low–high” variation. Spatially, there is an increasing trend from central Mongolia to Northeast China, and a decreasing trend to the east of Lake Baikal for genesis and passage, indicating that the tracks of Mongolian ETCs shift southward.

The opposite trends of ETC genesis and passage indicate that there may be different categories of Mongolian ETCs. Previous studies have also explored the classification of Mongolian ETCs (Zhang et al. 2012; Fu et al. 2013; Huang et al. 2016; Wang et al. 2024). For instance, Fu et al. (2013) classified Mongolian ETCs into six categories based on the relative position (angle) of genesis and lysis: stable track, northward track, eastward track, southeastward track, and southward track. Besides, Huang et al. (2016) divided Mongolian ETCs into eastward tracks and southeast tracks based on the relative position between the genesis and track in a zonal band of 42.5°–55°N. Moreover, some studies (Zhang et al. 2012; Wang et al. 2024) have adopted K-means clustering to cluster ETCs, and the results revealed two or three categories over Mongolian region. However, only partial information on the ETC tracks (e.g., information on only the genesis, lysis or ETC tracks during the first 2 days) was used in these studies, not information on the entire track (lifetime). The approach used in previous studies not only excluded the track information of long-lifetime ETCs over 2 days but also ignored the track information of ETCs with lifetime shorter than 2 days. However, short lifetime ETCs account for a large proportion (Fig. 4a). Therefore, the approach used in previous studies might lead to uncertainties in ETC classification. In contrast, the classification method used in this paper utilizes track information throughout the entire lifetime of the ETC. Based on this method, the Mongolian ETCs are classified into three categories: southern track (ST, accounting for 53.4% of Mongolian ETCs) ETCs, northern track (NT, accounting for 43.8%) ETCs, and long track (LT, accounting for 2.8%) ETCs. The ST ETCs has a significant increasing trend, while the NT ETCs has a significant decreasing trend, resulting in a weak trend in the Mongolian ETCs. Furthermore, the ST ETCs experience an interdecadal increase in approximately 2004, and the NT ETCs experience an interdecadal decrease in approximately 1993, which contribute two interdecadal changes in Mongolian ETCs. In contrast, due to the limited number of LT ETCs, their contribution to Mongolian ETC variation is limited.

Moreover, our study indicates that the properties (lifetime, moving distance, moving speed and intensity) of Mongolian ETCs show significant decadal variability. Lee et al. (2020) discussed the spatial distributions of climatology

related to the lifetime, moving speed, and traveling distance of ETCs over East Asia. However, they did not analyze the temporal changes in the aforementioned properties. Wang et al. (2024) analyzed several properties of Mongolian ETCs; however, they did not analyze the lifetime, maximum moving speed, or maximum intensity, and they gave more attention to background circulations rather than changes in ETC properties in recent decades. We extend these studies in this paper, founding that the lifetime, moving distance, moving speed and intensity (Cslp and LPslp) of Mongolian ETCs experience a decadal abrupt change in the 1990s. After the abrupt change, the lifetime and moving distance increase, the moving speed increases, and the intensity increases significantly. Furthermore, the properties of the classified ETCs also show consistent changes.

Previous studies have suggested that baroclinicity and potential vorticity (PV) have significant impacts on the genesis and development of ETCs (Eady 1949; Tao et al. 2017; Lee et al. 2020; Madonna et al. 2020; Kang and Son 2021; Simmonds and Li 2021; Lin et al. 2023; Zhang et al. 2023; Kong et al. 2024). In terms of climatology (figure not shown), high Eady growth rate (EGR) values are mainly located in the central and western Mongolia (consistent with main genesis area of ST ETCs in Fig. 8a), and high PV tongue is located to the east of Lake Baikal (consistent with main genesis area of NT ETCs in Fig. 8b), which may affect the ETCs over the Mongolian region. To verify the conjecture, we conduct regression analysis (Fig. 13). As shown in Fig. 13a, there are significant positive EGR over Mongolia, indicating a close relationship between ST ETCs and EGR. The correlation coefficient between EGR index (EGRI, defined as the area-averaged EGR over the region of 45°–55°N, 80°–115°E) and ST frequency is 0.50 ($P < 0.01$). The EGRI shows a significant positive trend (0.013 day⁻¹ per decade, $P < 0.10$), which is consistent with the positive trend of ST ETCs (Fig. 9a). Due to EGR depends on both vertical wind shear (VWS, defined as zonal wind difference 500- and 850-hPa pressure levels) and bulk static stability (BSS, defined as potential temperature difference at the 500- and 850-hPa pressure levels), we also analyze the relationships between ST ETCs and VWS as well as BSS. The VWS also shows significant correlation with ST ETCs over the same region, and the correlation coefficient between VWS index (VWSI, defined as the area-averaged VWS over the region of 45°–55°N, 80°–115°E) and ST frequency is 0.38 ($P < 0.05$). However, BSS does not show significant signal related to ST ETCs (figure not shown). Thus, the connection between EGR and ST ETCs is mainly contributed by VWS. On the contrary, EGR and NT ETCs do not show a significant correlation (Fig. 13b), indicating that the changes in NT ETCs may be related to other factors. Figure 13f shows significant positive PV anomalies over the polar region to Mongolia for NT ETCs, indicating that the NT ETCs may

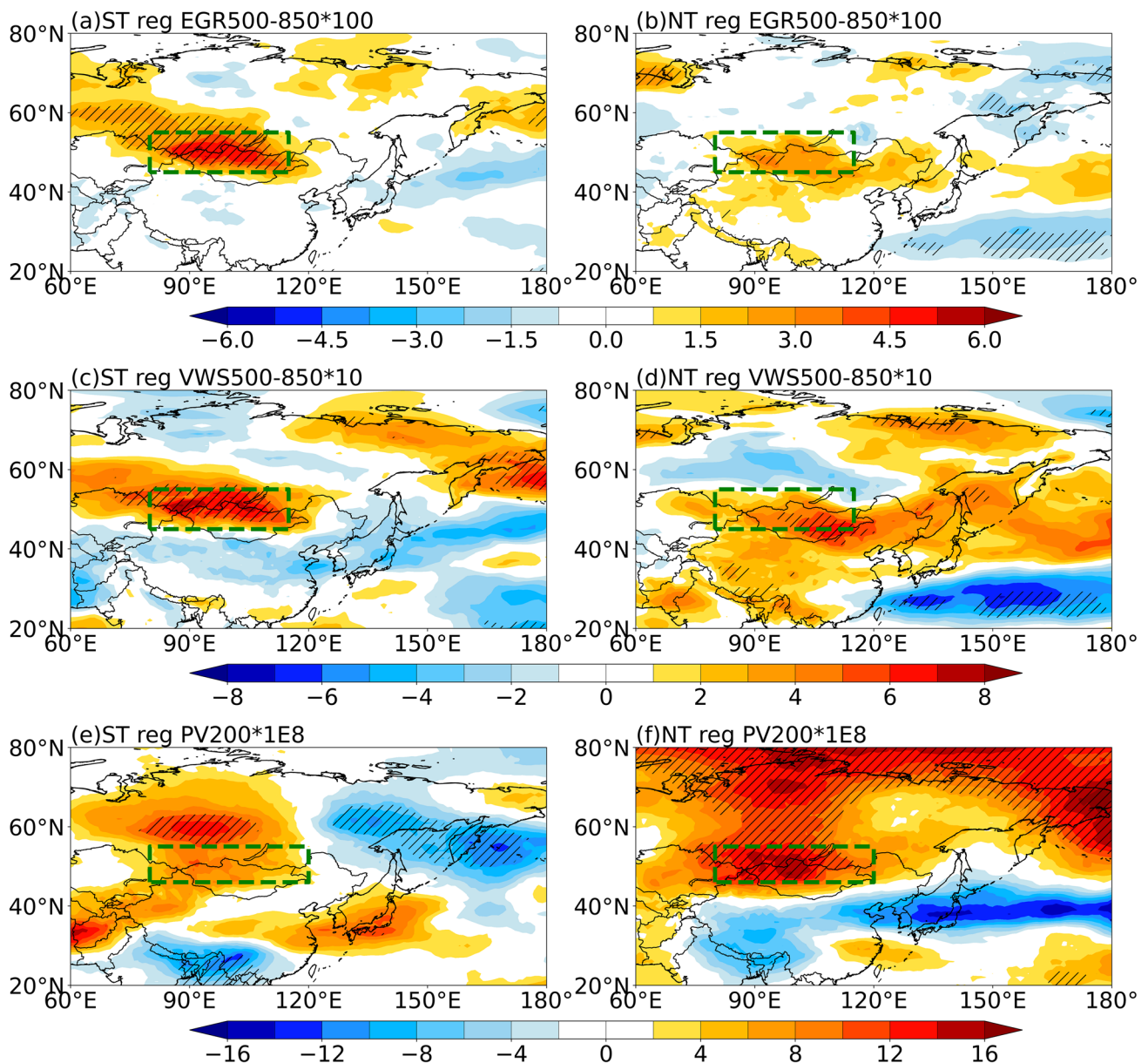


Fig. 13 Linear regressions of (a) EGR (unit: $\times 10^{-2} \text{ day}^{-1}$), (c) VWS (unit: 10 m s^{-1}), and (e) 200-hPa potential vorticity (unit: $\times 10^{-8} \text{ K m}^2 \text{ kg}^{-1} \text{ s}^{-1}$) against the standardized ST frequency in spring during 1979–2021. (b, d, f) Same as (a, c, e), but against the

standardized NT frequency. Slant lines indicate regions over which the regression coefficients are significant at $P < 0.05$. The green dashed boxes represent the indices definition areas

be closely related to the downward transmission of PV from high-latitude. The significant signals in the polar region also indicate that these PV anomalies are likely to come from the Arctic vortex, and further detailed study is needed. Defining the average PV in the green box (46° – 55°N , 80° – 120°E) in Fig. 13f as the PV index (PVI), we can get significant correlation of the index with NT frequency (with correlation coefficient of 0.38, $P < 0.05$). The PVI shows a significant negative trend ($-8.62 \times 10^{-8} \text{ K m}^2 \text{ kg}^{-1} \text{ s}^{-1}$ per decade, $P < 0.05$), which is consistent with the negative trend of NT

ETCs (Fig. 9b). Conversely, PV does not show significant signals related to ST ETCs (Fig. 13e). The above results indicate that ST ETCs could be mainly affected by baroclinicity, while NT ETCs could be more affected by PV.

However, the above discussion is mainly about the role of atmospheric internal variability on ETCs. Along with the global warming, climate change exerts significant impact on atmospheric systems (including ETCs). For example, some studies reported that the ETC frequency in Northern Hemisphere mid-latitude may decrease in a warming climate

(Pinto et al. 2007; Chang et al. 2012; Zappa et al. 2013; Lee et al. 2022). Our results show that the ST ETCs have a significant increasing trend and NT ETCs have a significant decreasing trend, which could be mainly affected by EGR and PV, respectively. Due to the non-uniformity of global warming, the EGR and PV may undergo changes (e.g. Simmonds and Li 2021; Lee et al. 2022), which could affect ETCs. Therefore, it is necessary to conduct systematic studies on detection and attribution analysis to explain the impact of climate change on ETCs in the future.

Acknowledgements This work was supported by the National Natural Science Foundation of China (Grant No. 42221004). The authors are grateful to the Melbourne University for their cyclone detection and tracking algorithm.

Author contributions Conceptualization: [Jianqi Sun]; Data curation: [Kai Wang]; Formal analysis and investigation: [Jianqi Sun], [Kai Wang]; Funding acquisition: [Jianqi Sun]; Methodology: [Kai Wang]; Software: [Kai Wang]; Supervision: [Jianqi Sun]; Visualization: [Kai Wang]; Writing—original draft preparation: [Kai Wang], [Jianqi Sun], [Yanbo Nie]; Writing—review and editing: [Jianqi Sun].

Funding This work was supported by the National Natural Science Foundation of China (Grant No. 42221004).

Data availability The ERA5 reanalysis dataset can be downloaded from <https://climate.copernicus.eu/climate-reanalysis>. The HadSLP2 dataset are available at <https://www.metoffice.gov.uk/hadobs/hadslp2>.

Declarations

Conflict of interest The authors have no competing interests to declare that are relevant to the content of this article.

References

- Adachi S, Kimura F (2007) A 36-year climatology of surface cyclogenesis in East Asia using high-resolution reanalysis data. *Sola* 3:113–116. <https://doi.org/10.2151/sola.2007-029>
- Allan R, Ansell T (2006) A new globally complete monthly historical gridded mean sea level pressure dataset (HadSLP2): 1850–2004. *J Clim* 19:5816–5842. <https://doi.org/10.1175/JCLI3937.1>
- Bueh C, Zhuge A, Xie Z et al (2022) The development of a powerful Mongolian cyclone on 14–15 March 2021: Eddy energy analysis. *Atmospheric Ocean Sci Lett* 15:44–51. <https://doi.org/10.1016/j.aosl.2022.100259>
- Caliński T, Harabasz J (1974) A dendrite method for cluster analysis. *Commun Stat* 3:1–27. <https://doi.org/10.1080/03610927408827101>
- Catto JL (2018) A new method to objectively classify extratropical cyclones for climate studies: testing in the southwest Pacific region. *J Clim* 31:4683–4704. <https://doi.org/10.1175/JCLI-D-17-0746.1>
- Chang EKM, Lee S, Swanson KL (2002) Storm track dynamics. *J Clim* 15:2163–2183. [https://doi.org/10.1175/1520-0442\(2002\)015%3c02163:STD%3e2.0.CO;2](https://doi.org/10.1175/1520-0442(2002)015%3c02163:STD%3e2.0.CO;2)
- Chang EKM, Guo Y, Xia X (2012) CMIP5 multimodel ensemble projection of storm track change under global warming. *J Geophys Res Atmos*. <https://doi.org/10.1029/2012JD018578>
- Chen S-J, Kuo Y-H, Zhang P-Z, Bai Q-F (1991) Synoptic climatology of cyclogenesis over East Asia, 1958–1987. *Mon Weather Rev* 119:1407–1418. [https://doi.org/10.1175/1520-0493\(1991\)119%3c1407:SCOCOE%3e2.0.CO;2](https://doi.org/10.1175/1520-0493(1991)119%3c1407:SCOCOE%3e2.0.CO;2)
- Chen H, Teng F, Zhang W, Liao H (2017) Impacts of anomalous midlatitude cyclone activity over East Asia during summer on the decadal mode of East Asian summer monsoon and its possible mechanism. *J Clim* 30:739–753. <https://doi.org/10.1175/JCLI-D-16-0155.1>
- Chung Y-S, Hage KD, Reinelt ER (1976) On lee cyclogenesis and airflow in the Canadian Rocky Mountains and the East Asian mountains. *Mon Weather Rev* 104:879–891. [https://doi.org/10.1175/1520-0493\(1976\)104%3c0879:OLCAAI%3e2.0.CO;2](https://doi.org/10.1175/1520-0493(1976)104%3c0879:OLCAAI%3e2.0.CO;2)
- Crawford AD, Schreiber EAP, Sommer N et al (2021) Sensitivity of Northern Hemisphere cyclone detection and tracking results to fine spatial and temporal resolution using ERA5. *Mon Weather Rev* 149:2581–2598. <https://doi.org/10.1175/MWR-D-20-0417.1>
- Eady ET (1949) Long waves and cyclone waves. *Tellus* 1:33–52. <https://doi.org/10.3402/tellusa.v1i3.8507>
- Fu J, Dong L, Kang Z (2013) Climatology and interannual variability of extratropical cyclones in the winter half-year in northern China (in Chinese). *Chin J Atmos Sci* 37:679–690
- Hawcroft MK, Shaffrey LC, Hodges KI, Dacre HF (2012) How much Northern Hemisphere precipitation is associated with extratropical cyclones? *Geophys Res Lett* 39:L24809. <https://doi.org/10.1029/2012GL053866>
- Hersbach H, Bell B, Berrisford P et al (2020) The ERA5 global reanalysis. *Q J R Meteorol Soc* 146:1999–2049. <https://doi.org/10.1002/qj.3803>
- Hirata H (2021) Climatological features of strong winds caused by extratropical cyclones around Japan. *J Clim* 34:4481–4494. <https://doi.org/10.1175/JCLI-D-20-0577.1>
- Hodges KI (1995) Feature tracking on the unit sphere. *Mon Weather Rev* 123:3458–3465. [https://doi.org/10.1175/1520-0493\(1995\)123%3c3458:FTOTUS%3e2.0.CO;2](https://doi.org/10.1175/1520-0493(1995)123%3c3458:FTOTUS%3e2.0.CO;2)
- Hodges KI, Hoskins BJ, Boyle J, Thorncroft C (2003) A comparison of recent reanalysis datasets using objective feature tracking: storm tracks and tropical easterly waves. *Mon Weather Rev* 131:2012–2037. [https://doi.org/10.1175/1520-0493\(2003\)131%3c2012:ACORRD%3e2.0.CO;2](https://doi.org/10.1175/1520-0493(2003)131%3c2012:ACORRD%3e2.0.CO;2)
- Hoskins BJ, Hodges KI (2002) New perspectives on the Northern Hemisphere winter storm tracks. *J Atmospheric Sci* 59:1041–1061. [https://doi.org/10.1175/1520-0469\(2002\)059%3c1041:NPOTNH%3e2.0.CO;2](https://doi.org/10.1175/1520-0469(2002)059%3c1041:NPOTNH%3e2.0.CO;2)
- Huang X, Bueh C, Xie Z, Gong Y (2016) Mongolian cyclones that influence the northern part of China in spring and their associated low-frequency background circulations (in Chinese). *Chin J Atmos Sci* 40:489–503
- Jin S, Feng S, Liu X et al (2021) On the formation and wind enhancement mechanisms of a Mongolian cyclone that caused a transmission line galloping trip in Gansu province. *Atmospheric Ocean Sci Lett* 14:100022. <https://doi.org/10.1016/j.aosl.2020.100022>
- Kang JM, Son S-W (2021) Development processes of the explosive cyclones over the northwest Pacific: potential vorticity tendency inversion. *J Atmospheric Sci* 78:1913–1930. <https://doi.org/10.1175/JAS-D-20-0151.1>
- Kong Y, Lu C, Guan Z, Chen X (2024) Comparison of intense summer Arctic cyclones between the marginal ice zone and central Arctic. *J Geophys Res Atmospheres* 129(3):e2023JD039620. <https://doi.org/10.1029/2023JD039620>
- Lee J, Son S-W, Cho H-O et al (2020) Extratropical cyclones over East Asia: climatology, seasonal cycle, and long-term trend. *Clim Dyn* 54:1131–1144. <https://doi.org/10.1007/s00382-019-05048-w>

- Lee J, Hwang J, Son S-W, Gyakum JR (2022) Future changes of East Asian extratropical cyclones in the CMIP5 models. *J Clim* 35:6911–6921. <https://doi.org/10.1175/JCLI-D-21-0945.1>
- Li W-L, Xia R-D, Sun J-H et al (2019) Layer-wise formation mechanisms of an entire-troposphere-thick extratropical cyclone that induces a record-breaking catastrophic rainstorm in Beijing. *J Geophys Res Atmos* 124:10567–10591. <https://doi.org/10.1029/2019JD030868>
- Lin D, Huang W, Yang Z et al (2019) Impacts of wintertime extratropical cyclones on temperature and precipitation over Northeastern China during 1979–2016. *J Geophys Res Atmos* 124:1514–1536. <https://doi.org/10.1029/2018JD029174>
- Lin P, Zhong R, Yang Q et al (2023) A record-breaking cyclone over the Southern Ocean in 2022. *Geophys Res Lett* 50:e2022GL104012. <https://doi.org/10.1029/2023GL104012>
- Madonna E, Hes G, Li C et al (2020) Control of Barents Sea wintertime cyclone variability by large-scale atmospheric flow. *Geophys Res Lett* 47:e2020GL090322. <https://doi.org/10.1029/2020GL090322>
- Mann HB, Whitney DR (1947) On a test of whether one of two random variables is stochastically larger than the other. *Ann Math Stat* 18:50–60. <https://doi.org/10.1214/aoms/1177730491>
- Messmer M, Simmonds I (2021) Global analysis of cyclone-induced compound precipitation and wind extreme events. *Weather Clim Extrem* 32:100324. <https://doi.org/10.1016/j.wace.2021.100324>
- Murray RJ, Simmonds I (1991) A numerical scheme for tracking cyclone centres from digital data. Part I: development and operation of the scheme. *Aust Meteorol Mag* 39:155–166
- Nakamura J, Lall U, Kushnir Y, Camargo SJ (2009) Classifying north Atlantic tropical cyclone tracks by mass moments. *J Clim* 22:5481–5494. <https://doi.org/10.1175/2009JCLI2828.1>
- Neu U, Akperov MG, Bellenbaum N et al (2013) IMILAST: A community effort to intercompare extratropical cyclone detection and tracking algorithms. *Bull Am Meteorol Soc* 94:529–547. <https://doi.org/10.1175/BAMS-D-11-00154.1>
- Nie Y, Sun J (2022) Moisture sources and transport for extreme precipitation over Henan in July 2021. *Geophys Res Lett* 49:e2021GL097446. <https://doi.org/10.1029/2021GL097446>
- Owen LE, Catto JL, Stephenson DB, Dunstone NJ (2021) Compound precipitation and wind extremes over Europe and their relationship to extratropical cyclones. *Weather Clim Extrem* 33:100342. <https://doi.org/10.1016/j.wace.2021.100342>
- Papritz L, Pfahl S, Rudeva I et al (2014) The role of extratropical cyclones and fronts for southern ocean freshwater fluxes. *J Clim* 27:6205–6224. <https://doi.org/10.1175/JCLI-D-13-00409.1>
- Pezza AB, Durrant T, Simmonds I, Smith I (2008) Southern Hemisphere synoptic behavior in extreme phases of SAM, ENSO, sea ice extent, and southern Australia rainfall. *J Clim* 21:5566–5584. <https://doi.org/10.1175/2008JCLI2128.1>
- Pfahl S, Sprenger M (2016) On the relationship between extratropical cyclone precipitation and intensity. *Geophys Res Lett* 43:1752–1758. <https://doi.org/10.1002/2016GL068018>
- Pinto JG, Spanghel T, Ulbrich U, Speth P (2005) Sensitivities of a cyclone detection and tracking algorithm: individual tracks and climatology. *Meteorol Z* 14:823–838. <https://doi.org/10.1127/0941-2948/2005/0068>
- Pinto JG, Ulbrich U, Leckebusch GC et al (2007) Changes in storm track and cyclone activity in three SRES ensemble experiments with the ECHAM5/MPI-OM1 GCM. *Clim Dyn* 29:195–210. <https://doi.org/10.1007/s00382-007-0230-4>
- Qian W, Quan L, Shi S (2002) Variations of the dust storm in China and its climatic control. *J Clim* 15:1216–1229. [https://doi.org/10.1175/1520-0442\(2002\)015%3c1216:VOTDSI%3e2.0.CO;2](https://doi.org/10.1175/1520-0442(2002)015%3c1216:VOTDSI%3e2.0.CO;2)
- Reale M, Liberato MLR, Lionello P et al (2019) A global climatology of explosive cyclones using a multi-tracking approach. *Tellus Dyn Meteorol Oceanogr* 71:1611340. <https://doi.org/10.1080/16000870.2019.1611340>
- Rudeva I, Gulev SK, Simmonds I, Tilinina N (2014) The sensitivity of characteristics of cyclone activity to identification procedures in tracking algorithms. *Tellus Dyn Meteorol Oceanogr* 66:24961. <https://doi.org/10.3402/tellusa.v66.24961>
- Simmonds I, Li M (2021) Trends and variability in polar sea ice, global atmospheric circulations, and baroclinicity. *Ann N Y Acad Sci* 1504:167–186. <https://doi.org/10.1111/nyas.14673>
- Simmonds I, Murray RJ, Leighton RM (1999) A refinement of cyclone tracking methods with data from FROST. *Aust Meteorol Mag* 48:35–49
- Sinclair MR (1997) Objective identification of cyclones and their circulation intensity, and climatology. *Weather Forecast* 12:595–612. [https://doi.org/10.1175/1520-0434\(1997\)012%3c0595:OIOCAT%3e2.0.CO;2](https://doi.org/10.1175/1520-0434(1997)012%3c0595:OIOCAT%3e2.0.CO;2)
- Takemi T, Seino N (2005) Dust storms and cyclone tracks over the arid regions in East Asia in spring. *J Geophys Res Atmospheres* 110:D18S11. <https://doi.org/10.1029/2004JD004698>
- Tamura K, Sato T (2022) Decrease of winter cyclone passage over northern Japan due to the reduction in the regional cyclogenesis associated with cold air outbreak. *Int J Climatol* 42:7598–7610. <https://doi.org/10.1002/joc.7667>
- Tao W, Zhang J, Zhang X (2017) The role of stratosphere vortex downward intrusion in a long-lasting late-summer Arctic storm. *Q J R Meteorol Soc* 143:1953–1966. <https://doi.org/10.1002/qj.3055>
- Ulbrich U, Leckebusch GC, Grieger J et al (2013) Are greenhouse gas signals of Northern Hemisphere winter extra-tropical cyclone activity dependent on the identification and tracking algorithm? *Meteorol Z* 22:61–68. <https://doi.org/10.1127/0941-2948/2013/0420>
- Ullrich PA, Zarzycki CM (2017) TempestExtremes: a framework for scale-insensitive pointwise feature tracking on unstructured grids. *Geosci Model Dev* 10:1069–1090. <https://doi.org/10.5194/gmd-10-1069-2017>
- Ullrich PA, Zarzycki CM, McClenny EE et al (2021) TempestExtremes v2.1: a community framework for feature detection, tracking, and analysis in large datasets. *Geosci Model Dev* 14:5023–5048. <https://doi.org/10.5194/gmd-14-5023-2021>
- Varino F, Arbogast P, Joly B et al (2019) Northern Hemisphere extratropical winter cyclones variability over the 20th century derived from ERA-20C reanalysis. *Clim Dyn* 52:1027–1048. <https://doi.org/10.1007/s00382-018-4176-5>
- Wang R (1963) The tracks of the extratropical cyclones in eastern Asia (in Chinese). *Acta Meteorol Sin* 33:15–24
- Wang X, Zhai P, Wang C (2009) Variations in extratropical cyclone activity in northern East Asia. *Adv Atmospheric Sci* 26:471–479. <https://doi.org/10.1007/s00376-009-0471-8>
- Wang XL, Feng Y, Chan R, Isaac V (2016) Inter-comparison of extratropical cyclone activity in nine reanalysis datasets. *Atmospheric Res* 181:133–153. <https://doi.org/10.1016/j.atmosres.2016.06.010>
- Wang J, Chen L, Li S (2024) Characteristics of spring Mongolian cyclones in the recent 70 years: background circulations and weather influences. *Int J Climatol* 44:328–343. <https://doi.org/10.1002/joc.8342>
- Wernli H, Schwierz C (2006) Surface cyclones in the ERA-40 dataset (1958–2001). Part I: novel identification method and global climatology. *J Atmospheric Sci* 63:2486–2507. <https://doi.org/10.1175/JAS3766.1>
- Whittaker LM, Horn LH (1984) Northern Hemisphere extratropical cyclone activity for four mid-season months. *J Climatol* 4:297–310. <https://doi.org/10.1002/joc.3370040307>
- Wu X, Tan X, Liu B et al (2022) Fronts and cyclones associated with changes in the total and extreme precipitation over China. *J Clim* 35:4131–4146. <https://doi.org/10.1175/JCLI-D-21-0467.1>
- Yang M, Luo D, Li C et al (2021) Inconsistent variations between the northern and southern North Pacific storm track. *Geophys Res Lett* 48:e2021GL095552. <https://doi.org/10.1029/2021GL095552>

- Yao S, Zhang Y, Zhou T (2003) Climatic characteristics of extratropical cyclone frequency and its variations over East Asia during recent 50 years in spring (in Chinese). *J Nanjing Inst Meteorol* 26:317–323
- Yin Z, Wan Y, Zhang Y, Wang H (2022) Why super sandstorm 2021 in North China? *Natl Sci Rev* 9:nwab165. <https://doi.org/10.1093/nsr/nwab165>
- Yu B, Wang XL, Feng Y et al (2022) Northern Hemisphere extratropical cyclone activity in the twentieth century reanalysis version 3 (20CRv3) and its relationship with continental extreme temperatures. *Atmosphere* 13:1166. <https://doi.org/10.3390/atmos13081166>
- Zappa G, Shaffrey LC, Hodges KI et al (2013) A multimodel assessment of future projections of north atlantic and european extratropical cyclones in the cmip5 climate models. *J Clim* 26:5846–5862. <https://doi.org/10.1175/JCLI-D-12-00573.1>
- Zhang Y, Ding Y, Li Q (2012) A climatology of extratropical cyclones over East Asia during 1958–2001. *Acta Meteorol Sin* 26:261–277. <https://doi.org/10.1007/s13351-012-0301-2>
- Zhang X, Tang H, Zhang J et al (2023) Arctic cyclones have become more intense and longer-lived over the past seven decades. *Commun Earth Environ* 4:1–12. <https://doi.org/10.1038/s43247-023-01003-0>
- Zhong R, Yang Q, Hodges K et al (2023) Impact of data resolution on tracking southern ocean cyclones. *Mon Weather Rev* 151:3–22. <https://doi.org/10.1175/MWR-D-22-0121.1>
- Zhu C, Wang B, Qian W (2008) Why do dust storms decrease in northern China concurrently with the recent global warming? *Geophys Res Lett* 35:L18702. <https://doi.org/10.1029/2008GL034886>

Publisher's Note Springer Nature remains neutral with regard to jurisdictional claims in published maps and institutional affiliations.

Springer Nature or its licensor (e.g. a society or other partner) holds exclusive rights to this article under a publishing agreement with the author(s) or other rightsholder(s); author self-archiving of the accepted manuscript version of this article is solely governed by the terms of such publishing agreement and applicable law.